Transcriptional alterations in opioid use disorder reveal an interplay between neuroinflammation and synaptic remodeling

Marianne L. Seney[1], Sam Moon-Kim[1,2,3], Jill R. Glausier[1], Mariah A. Hildebrand[1], Xiangning Xue[4], Wei Zong[4], Jiebiao Wang[4], Micah A. Shelton[1], BaDoi N. Phan[5], Chaitanya Srinivasan[5], Andreas R. Pfenning[5,6], George C. Tseng[4], David A. Lewis[1], Zachary Freyberg[1,7] and Ryan W. Logan[1,2,3]*

[1]Translational Neuroscience Program, Department of Psychiatry, University of Pittsburgh School of Medicine, Pittsburgh, PA 15219, USA.

[2]Center for Adolescent Reward, Rhythms, and Sleep, University of Pittsburgh, Pittsburgh, PA 15219, USA.

[3]Center for Systems Neurogenetics of Addiction, The Jackson Laboratory, Bar Harbor, ME 04609.

[4]Department of Biostatistics, University of Pittsburgh, Pittsburgh, PA 15261, USA.

[5]Department of Computational Biology, Carnegie Mellon University, Pittsburgh, PA 15213, USA.

[6]Neuroscience Institute, Carnegie Mellon University, Pittsburgh, PA 15213, USA.

[7]Department of Cell Biology, University of Pittsburgh, Pittsburgh, PA 15213, USA.

*To whom correspondence should be addressed:

Ryan W. Logan, PhD
Translational Neuroscience Program
Department of Psychiatry
University of Pittsburgh School of Medicine
450 Technology Drive, Office 224
Pittsburgh, PA 15219
loganrw@upmc.edu
412-383-3084

Abstract

Prevalence rates of opioid use disorder (OUD) have increased dramatically, accompanied by a surge of overdose deaths. While opioid dependence has been extensively studied in preclinical models, we still have a very limited understanding of the biological changes that occur in the brains of people who chronically use opioids and who are diagnosed with OUD. To address this, we conducted the largest transcriptomics study to date using postmortem brains from subjects with OUD. We focused on the dorsolateral prefrontal cortex (DLPFC) and nucleus accumbens (NAc), two regions heavily implicated in OUD. We discovered a high degree of overlap in transcripts between DLPFC and NAc in OUD, primarily associated with neuroinflammation. Moreover, additional transcripts were enriched for factors that control pro-inflammatory cytokine-mediated signaling and remodeling of the extracellular matrix (ECM). Our results also implicate a role for microglia as a critical driver for opioid-induced neuroplasticity. Overall, our findings reveal new connections between the brain's immune system and opioid dependence in the human brain.

50 **Introduction**

51 Prevalence of opioid use disorder (OUD) and deaths from opioid overdose have
52 soared in the United States, mainly fueled by the availability of highly potent synthetic
53 opioids(*1*). The enormity of the public health impact, along with high relapse rates(*2*), has
54 been the impetus for wide ranging efforts to develop new treatments for OUD. Progress
55 towards more effective therapeutics requires better understanding of the alterations that
56 occur in the brain of those who develop dependence.

57 Impulsivity and deficits in cognition are hallmarks of OUD(*3*). These impairments
58 have been attributed to functional alterations in corticostriatal circuits involving the
59 dorsolateral prefrontal cortex (DLPFC) and nucleus accumbens (NAc)(*4*). DLPFC—NAc
60 circuitry regulates cognitive and emotional states that guide reward-seeking(*3*).
61 Moreover, a history of substance use is associated with corticostriatal circuit dysfunction
62 that leads to cognitive impairment and further promotes risky behavior(*5*). The circuitry of
63 opioid dependence has been extensively studied in preclinical models. Yet, we still have
64 a limited understanding of the cellular and molecular changes that occur in these circuits
65 as a consequence of chronic opioid use and OUD in human brain.

66 Although few studies have investigated postmortem brains in OUD, this approach
67 has the potential to uncover clinically relevant pathways in opioid dependence. For
68 example, previous work showed changes in opioid receptor expression in the DLPFC
69 related to addiction severity in heroin users(*6-8*). Moreover, recent findings showed heroin
70 users have altered expression of the presynaptic machinery regulating glutamate release
71 in the NAc(*9,10*). Nevertheless, deeper knowledge into the molecular alterations to
72 opioids in the DLPFC and NAc is extremely limited.

We aimed to establish a more comprehensive understanding of the genetic, molecular, and cellular adaptations across DLPFC and NAc in the brains of human subjects who were chronic opioid users and also had an established diagnosis of OUD at time of death. To accomplish this, we used multiple levels of analysis by integrating transcriptomics across brain regions with behaviors related to OUD vulnerability by GWAS. Between the DLPFC and NAc, we found remarkable overlap in both upregulated and downregulated transcripts. Further investigation into these overlapping transcripts revealed pathways enriched for factors that control the formation and degradation of the extracellular matrix (ECM) and pro-inflammatory cytokine-mediated signaling. These pathways implicate neuroinflammation as a driver of ECM remodeling and synaptic reorganization, processes which are critical for opioid-induced neuroplasticity(*11*). Consistent with this, our analyses showed that microglia were central to these OUD effects in both the DLPFC and NAc. Different elements of these respective pathways are selectively enriched in DLPFC (*e.g.,* TNFα and NFκB signaling) and others in the NAc. Finally, we found direct links between neuroinflammation, risky behavior, and OUD using GWAS findings, which suggests novel genetic and molecular changes that may ultimately drive drug-seeking in OUD.

Results

Enrichment of differentially expressed transcripts involved in neuroinflammation and ECM remodeling in DLPFC and NAc in OUD

To our knowledge, we have assembled the largest sample size of subjects with OUD and matched controls (n=20 per group; Table 1 and table S1) across DLPFC and

96 NAc, both collected from the same subject. We examined whether there were
97 transcriptional differences by brain region in OUD. Our RNA-seq analyses in control
98 subjects showed that different brain regions had unique transcriptional profiles (Figure
99 S1). Many of the transcripts enriched in DLPFC were significantly related to synaptic
100 vesicle transport (*e.g., KIF5C*(*12,13*)*, STXBP5L*(*14*)), exocytosis (*e.g., STX1A*(*15*)), and
101 neurotransmitter release (*e.g,. CADPS2(16), RIMS3*(*17*)) (Data file S1). By comparison,
102 in the NAc, transcripts associated with cytoskeletal remodeling and chemotaxis regulation
103 were enriched (*e.g, ROBO1(18), MTUS1(19)*) (Data file S1).

104 We next investigated the potential impact of region-specific transcriptional
105 differences in OUD by comparing subjects with OUD to matched controls. We discovered
106 high numbers differentially expressed (DE) transcripts in both brain regions (567 in
107 DLPFC (Data file S2); 1306 in NAc (Data file S3); Table 2). Our results showed that opioid
108 dependence had a profound effect on gene expression in both DLPFC and NAc. The
109 volcano plot of DE results for the DLPFC revealed a relatively even spread between
110 transcripts that were downregulated (339 transcripts) or upregulated (228 transcripts) in
111 OUD subjects (Table 2, figure 1a, and data file S2). Control subjects were differentiated
112 from OUD subjects by unsupervised clustering based on the expression of the top 250
113 DE transcripts in DLPFC with the most robust $\log_2$FC (Figure 1b). The volcano plot of DE
114 results for the NAc revealed that a majority of the DE transcripts were downregulated
115 (1085 transcripts compared to 221 upregulated transcripts) in OUD subjects (Figure 1c
116 and data file S3). Unsupervised clustering of subjects based on the top 250 DE transcripts
117 in the NAc identified subgroups in both the control and OUD cohorts (Figure 1d).

118 To determine the identity of the genes encoded by these transcripts, we focused
119 on protein-coding and long noncoding RNAs (lncRNAs) because they were prominent in
120 both brain regions in OUD subjects. In DLPFC, 73.4% of DE transcripts were protein-
121 coding and 19.5% were lncRNAs (Figure 2a). We examined the functions of these DE
122 transcripts via pathway analysis. The top pathways represented by DE transcripts in the
123 DLPFC were tumor necrosis factor (TNFα) signaling via nuclear factor kappa B (NFκB),
124 as well as adipocytokine and interferon gamma signaling, clearly implicating an
125 inflammatory response in DLPFC in OUD (Figure 2b and figure S2). We also found
126 pathways related to vasculature and blood vessel development (Figure 2b and figure S2).

127 We then explored whether there was overlap of the top pathways identified above.
128 Indeed, our analyses indicated significant overlap between immune-related and vascular
129 pathways (Figure 2c). Using Ingenuity Pathway Analysis (IPA), we determined the top
130 upstream regulators predicted to be activated or inhibited based on their respective z-
131 scores. Consistent with enrichment of pro-inflammatory pathways, the top activated
132 upstream regulators in DLPFC were TNF, IL1B, and NFκB complex (Figure 2d).
133 Surprisingly, we discovered that all of the predicted upstream regulators that were
134 inhibited have key roles in the regulation of the vasculature, including KLF2(*20*),
135 NRAS(*21*), and PTEN(*22*) (Figure 2d). These findings suggest that vascular integrity may
136 be compromised in DLPFC of OUD subjects, in line with growing evidence that the blood
137 brain barrier (BBB) is eroded as consequence of repeated opioid use(*23,24*).

138 As a complementary approach to IPA, we used Hypergeometric Optimization of
139 Motif Enrichment (HOMER)(*25*) to predict transcription factors that may cause the
140 differential expression of transcripts in OUD. In DLPFC, the top transcription factors were

141 SRF, MEF2A, PKNOX1, PBX3, and SOX21 (Figure 2d). Each of these have roles in
142 neuronal survival(*26-34*), neuronal activation(*35,36*), synaptic plasticity(*27,28*), as well as
143 in inflammation(*37-39*).

144 Similar to DLPFC, the majority of DE transcripts in NAc were protein-coding
145 (89.5%), followed by lncRNAs (7.4%; Figure 2e). We found the top enriched pathways
146 were related to ECM, including those associated with chondroitin/dermatan sulfate
147 metabolism (Figure 2f). Intriguingly, our data suggests links between ECM remodeling,
148 microglial cell migration, and synaptic plasticity, in line with recent work(*40*). Specifically,
149 we discovered enrichment of pathways in synapse organization (Figure 2f, Figure S3).
150 We also found enrichment of ameboidal-type cell migration pathways (Figure 2f),
151 commonly used by activated microglia in response to neuroinflammation(*41*). Whereas
152 there was convergence of cooperative clusters of transcripts into a few, select final
153 common pathways in the DLPFC (Figure 2c), pathways in the NAc were largely discrete
154 (Figure 2g). Using IPA, we predicted the top upstream regulators either activated or
155 inhibited in NAc. The top activated upstream regulators were IL1B (activation of microglia
156 inflammatory response(*42*)), BRD7 (synaptic plasticity(*43*)), CREBBP (activity-dependent
157 synaptic remodeling and plasticity(*44*)), and OSM (cell-type dependent regulation of
158 myelination and inflammation(*45*)) (Figure 2h). While IKZF1 was predicted to be activated
159 in NAc, this regulator was predicted to be inhibited in DLPFC of OUD subjects, suggesting
160 opioids differentially impact IKZF1 activity and target transcripts in a region-specific
161 manner. Interestingly, IKZF1 is a master regulator of immune cell activation(*46-48*). The
162 top inhibited upstream regulators were UHRF2 (modulator of DNA methylation(*49*)), IgG
163 (Complex) (immunomodulation(*50*)), PTEN (vasculature integrity(*22,51*)), ZBTB16

164 (chromatin remodeling via histone deacetylation(*52,53*) including in response to drugs of
165 abuse(*54*)), and RB1 (cell survival and migration(*55*)).

166 As in DLPFC, we identified the top transcription factors using HOMER analysis in
167 NAc in OUD. We found several POU family transcription factors(*56*) (POU2F3, POU2F2,
168 and BRN1), which have critical roles in inflammation(*57-59*) and neurodevelopment(*60-*
169 *62*). Moreover, we identified the nuclear orphan receptor, RORα, which is also important
170 in neuroinflammation(*63-65*) (Figure 2h). While the DLPFC and NAc vary in how each
171 coordinate their respective signaling pathways, nevertheless, our data demonstrate that
172 both regions share common neuroinflammation and ECM pathways, suggesting the
173 importance of both in alterations related to chronic opioids.

174

175 *High transcriptional coherence between DLPFC and NAc converges on*
176 *neuroinflammatory and ECM pathways in OUD*

177 Because of the many shared pathways across brain regions in OUD, we
178 comprehensively mapped the extent of transcriptional overlap between the DLPFC and
179 NAc. Such analyses may provide critical insight into the functional alterations across
180 DLPFC—NAc circuits(*3,11,66-69*). To investigate overlap of alterations between regions,
181 we used Rank-Rank Hypergeometric Overlap (RRHO) analysis(*70,71*). Our threshold-
182 free approach ordered transcripts in each brain region by both the direction of their effect
183 size and p-value. RRHO revealed substantial transcriptional overlap in both upregulated
184 and downregulated transcripts between DLPFC and NAc (Figure 3a and Figure S4).
185 Given this transcriptional coherence, we examined the pathways enriched from DE
186 transcripts shared between regions. Indeed, there was a high level of overlapping DE

187 transcripts between brain regions, even using strict significance cutoffs (Figure 3b-c;
188 Fisher's exact test, $p<10^{-6}$). Across DLPFC and NAc, the top shared pathways included
189 those related to ECM (*e.g.,* biosynthesis of glycosaminoglycans and chondroitin sulfate)
190 and neuroinflammation (*e.g.,* cytokine-mediated immune signaling via TNFα and NFκB)
191 (Figure 3d). Other enriched pathways were associated with cellular stress responses
192 (*e.g.,* DNA damage repair), as well as protein and histone modifications (*e.g.,*
193 ubiquitination and acetylation) that govern epigenetic regulation (Figure 3d and figure S5).

194 Our findings implicate epigenetic changes as a potential driver of transcriptional
195 alterations in OUD. Using genome-wide maps of epigenetic modifications derived from
196 human brain(*72*), we investigated the enrichment of chromatin state by comparing the
197 transcription start sites from DE transcripts in OUD to states previously defined in control
198 subjects(*72*). In DLPFC, we discovered that transcription start sites of DE transcripts were
199 enriched for genomic regions marked by weak polycomb repression at baseline (Figure
200 S6a, $p < 10^{-5}$). Weak polycomb repression diminishes histone marks (*e.g.,* H3K27me3),
201 which would otherwise inhibit transcription at the start site(*72*). Relative to baseline, the
202 enrichment of upregulated DE transcripts in DLPFC from OUD subjects suggests that
203 opioids induce the activation of otherwise repressed areas of the genome to promote
204 transcription (Figure S6). In NAc, we discovered DE transcripts were enriched for
205 genomic regions marked for a quiescent state at baseline ($p < 10^{-6}$; Figure S6a).
206 Quiescent states are characterized by the complete absence of histone marks linked to
207 transcriptional inactivity(*72*). Similar to DLPFC, such findings suggest opioids activate
208 otherwise inactive genomic regions, resulting in transcriptional upregulation in NAc

209 (Figure S6b). Overall, these findings reflect a fundamental disturbance of chromatin
210 states and transcriptional regulation by opioids relative to baseline epigenetic states.

211

212 *Upregulation of microglia markers in OUD*

213 Since we discovered high transcriptional coherence between DLPFC and NAc
214 (Figure 3a,b), we identified the cell types that specific DE transcripts were largely
215 expressed in from both brain regions via deconvolution analyses(*73*). We clustered
216 transcripts in major cell types in the brain including astrocytes, endothelial cells, microglia,
217 neurons, as well as oligodendrocytes and oligodendrocyte precursor cells. Relative to
218 control subjects, we found significant enrichment of microglial markers (*e.g.*, *ZNF812*) in
219 OUD (p=0.03; Figure 4a). This supports our evidence for neuroinflammatory processes
220 in DLPFC and NAc in OUD.

221 We next conducted cell type-specific DE analysis in DLPFC and NAc. We tested
222 each cell type from above to identify DE transcripts that significantly co-vary with the cell
223 type-specific markers. Using brain region as a covariate, we detected a single DE
224 transcript associated with microglia markers, *HSD17B14* (Table S2). Previous work
225 showed that reduced expression of *HSD17B14* in microglia resulted in exaggerated pro-
226 inflammatory glial activation(*74*).

227 Focusing on transcripts that correlated with changes in neuronal markers, we
228 identified 25 DE transcripts that were significantly enriched for pathways related to
229 neuroimmune signaling between neurons and local inflammatory cells (*e.g.,* microglia)
230 (Figure 4b and table S2). We found a number of upregulated genes that are controlled by

231 a single microRNA (miR), miR223 (Figure 4b). Importantly, miR223 is a crucial modulator
232 of macrophage activation(*39*), further implicating a role for microglia in the regulation of
233 neuroimmune responses in OUD. A broader view of these pathways indicated that
234 immune-related pathways were largely distinct between microglia and other immune cell
235 types including $CD4^+$ and $CD8^+$ T-cells (Figure 4c). This highlights the possibility of
236 interactions between neurons and multiple immune cell types in the brains of OUD
237 subjects. Lastly, we found strong enrichment of DE transcripts with synapse-related
238 pathways (Figure S7).

239

240 *Increased connectivity of neuroinflammatory and ECM signaling gene modules in OUD*

241 We used weighted gene co-expression network analysis (WGCNA) to investigate
242 correlational patterns among transcripts, and thus identify transcript modules involved in
243 OUD. WGCNA generated transcript co-expression networks in DLPFC and NAc from
244 both control and OUD subjects, identifying 17 co-expression modules in DLPFC and 15
245 modules in NAc (Figure 5a). To determine whether modules were specific to OUD, we
246 used module differential connectivity (MDC) analysis to directly compare the correlational
247 patterns (*i.e.*, connectivity) among transcripts of each module between OUD and control
248 subjects. More coordinated expression of transcripts in controls relative to OUD indicates
249 a 'gain' of connectivity in control subjects. Conversely, a module that loses connectivity
250 in controls is more coordinated in OUD than in controls. In DLPFC, 15 of 17 modules lost
251 connectivity and two remained unchanged in control subjects (Figure 5b). In NAc, 13 of
252 15 modules lost connectivity, while one module gained connectivity, and another

253 remained unchanged in controls (Figure 5b). These findings indicate that overall module
254 structures were largely distinct between OUD and control subjects.

255 To further investigate the biological significance of modules in OUD, we examined
256 the enrichment of DE transcripts within each module focused on mRNA and lncRNA
257 transcripts that were highly represented in DLPFC (Figure 2a) and NAc (Figure 2e). We
258 specifically concentrated on the DLPFC blue module and the NAc forestgreen module
259 because: 1) these modules had increased connectivity in OUD subjects compared to the
260 other modules, and 2) these modules were highly enriched for both DE mRNA and
261 lncRNA transcripts in OUD (DLPFC blue full DE list $q<10^{-26}$, mRNA $q<10^{-23}$, lncRNA
262 $p=0.002$; NAc forestgreen full DE list $q<10^{-23}$, mRNA $q<10^{-22}$, lncRNA $p=0.004$). The
263 topography of DLPFC blue and NAc forestgreen networks were markedly different in OUD
264 relative to control subjects (Figure 5e,f). In OUD, these networks were more correlated,
265 consistent with strengthening of module connectivity.

266 Given our previous findings of overlap in DE transcripts and pathways across
267 DLPFC and NAc, we next tested the degree of overlap in transcript co-expression
268 networks between DLPFC blue and NAc forestgreen modules. Indeed, there was
269 substantial overlap in transcripts between these modules (Fisher's exact test, $p<10^{-16}$).
270 We further examined the functions of the pathways shared between these modules. Our
271 analyses revealed pathways related to neuroinflammation and ECM remodeling,
272 consistent with our earlier findings (Figure 5d). The top shared pathways include TNFα
273 signaling via NFκB, interferon-γ response, and acute inflammatory response via IL-6(*75*)
274 and IL-2(*76*) signaling (Figure 5d and figure S8). We specifically identified upstream
275 regulators of these pathways. Significantly, all of the top shared regulators are modulators

276 of inflammatory response: PPARγ(*77*), NFKB1(*78*), RELA(*78*), STAT1(*79*), and SP1(*80*)
277 (Figure 5d). Notably, we also uncovered strong signal corresponding to pathways related
278 to ECM regulation and organization (Figure 5d). These data build upon our above
279 analyses highlighting critical roles for neuroinflammation and ECM in OUD.

280 To identify key drivers of transcriptional co-expression networks described above,
281 we used hub gene network analysis. Hubs are highly connected genes within a module
282 predicted to control expression of other module genes. Therefore, identifying OUD-
283 specific hubs offers putative mechanisms for how these transcriptional networks are
284 regulated in brains from subjects with OUD. A number of hub genes were distinct to OUD
285 in DLPFC and NAc. Several of these hub genes in DLPFC are involved in inflammatory
286 signaling, including *JAK3(81), SERPINB1(82),* and *RELL1* (*83*)(Figure 5f). In NAc, we
287 similarly found numerous hub genes involved in inflammation such as *TLR2(84),*
288 *TNFRSF10B(85),* and *NFIL3(86)* (Figure 5f).

289 We investigated whether additional classes of transcriptional regulators were also
290 highly connected within our co-expression networks including lncRNAs and genes
291 encoding RNA-binding proteins. Indeed, several lncRNAs were highly connected in co-
292 expression networks specific to OUD in DLPFC and NAc (*e.g.,* DLPFC: *AC0101086.3*
293 and NAc: *BAALC.AS1*) (Figure 5f and table S3). *AC0101086.3* is located proximal to
294 *CLEC2D* in the genome*,* another OUD-specific hub gene. Notably, *CLEC2D* encodes
295 ELT1, an activator of innate immune responses(*87,88*). *BAALC.AS1* is highly expressed
296 in brain and regulates astrocyte proliferation and differentation(*89*). In the NAc
297 forestgreen module, we also identified a transcript encoding the RNA-binding protein,
298 YBX3. YBX3 regulates the expression of the large neutral amino acid transporter 1

299 (LAT1)(*90*), which is necessary for the uptake of catecholamine precursor, L-DOPA in
300 dopaminergic cells(*91*). Interestingly, changes in the expression of *YBX3* in human
301 midbrain has previously been implicated in opioid dependence(*92*). Together, our data
302 provides further evidence that there are direct associations between neuroinflammation
303 and OUD.

304

305 *Associations between transcriptional alterations in the NAc and increased genetic liability*
306 *for substance use-related traits in OUD*

307 Opioid dependence is strongly linked to impulsive, risky behaviors. Given our
308 results highlighting inflammatory pathways in OUD, we sought to determine whether
309 these pathways were linked to traits related to opioid dependence. To test this, we
310 employed a GWAS-based approach that integrated risk loci associated with opioid
311 dependence and risky behavior(*93-95*) with transcriptional profiles in DLPFC and NAc
312 from OUD subjects. Loci identified by GWAS are known to overlap with intronic and distal
313 intergenic noncoding regions within *cis*-acting regulators of gene expression(*72*). Using
314 this information, we examined whether noncoding regions proximal to our DE transcripts
315 were enriched for genetic risk variants of both opioid dependence and risky behavior. We
316 found significant enrichment of downregulated DE transcripts in NAc of OUD subjects for
317 risky behavior GWAS (FDR<0.05; Figure S9a). Many of these transcripts were associated
318 with neuroimmune signaling, along with the machinery involved in synaptic
319 neurotransmission (Figures 2 and 5). There was no enrichment of DE transcripts in
320 chronic pain, opioid dependence, or unrelated GWAS traits (*i.e.,* bone mineral density,

321 coronary artery disease, and lean body mass) (Figure S9b,c). Our results therefore bridge
322 substance use related genetic risk factors to our gene expression findings in OUD.

323

324 **Discussion**

325 Our work demonstrates that inflammation is the most salient biological process
326 identified across our analyses in brains of subjects with OUD. This is consistent with
327 accumulating evidence from both human and animal studies that suggests inflammatory
328 processes are critical modulators of opioid reward and dependence. Clinical findings that
329 directly link inflammation to OUD come primarily from studies reporting elevated levels of
330 pro-inflammatory cytokines in the periphery of opioid dependent individuals(*96*).
331 Activation of pro-inflammatory cytokines in periphery and brain may have functional
332 consequences that contribute to OUD. In line with this, pharmacological inhibition of
333 activated microglia(*97*) mitigates subjective withdrawal(*98*) and reduces motivation to
334 consume opioids in dependent individuals(*99*). Similarly, glial inhibition attenuates opioid
335 conditioned reward and seeking behaviors in rodents(*100-103*). Furthermore, altered
336 dopaminergic and glutamatergic neurotransmission is implicated in both inflammation
337 and opioids(*96,104*), suggesting interactions between these pathways(*100,101,105-107*).
338 However, the unanswered question is whether these findings are clinically relevant for
339 OUD. To address this, we focused exclusively on the DLPFC and NAc, key regions
340 involved in OUD(*3*).

341 Across multiple levels of analysis, our results reveal several key inflammatory
342 pathways altered in OUD in both brain regions. One of the top shared pathways between
343 DLPFC and NAc is TNFα signaling via NFκB. Receptors known to activate NFκB, TNF

344 and TLR4(*108,109*), are among the top predicted upstream regulators of DE transcripts.
345 Upon activation, NFκB dimers translocate to the nucleus to drive transcription of immune-
346 related factors, including cytokines, chemokines, and interleukins(*108,109*), forming a
347 positive feedback loop that drives inflammation. In addition to its classical role in innate
348 immunity, opioids can activate NFκB signaling via opioid receptors(*110-114*). Activation
349 of NFκB signaling can, in turn, promote transcription of opioid receptors and
350 peptides(*115-120*), which may be involved in opioid reward and
351 dependence(*115,121,122*). Thus, while opioids can influence immune function via NFκB,
352 opioids may also activate NFκB, with downstream effects on addiction-related behaviors,
353 independent of immune function.

354 We also discovered inflammatory pathways altered by OUD that were distinct to
355 DLPFC. In DLPFC of OUD subjects, interferon-γ response was among the top enriched
356 pathways. In brain, interferon-γ is secreted by T helper cells, cytotoxic T lymphocytes,
357 and natural killer cells, that activate local microglia to initiate an inflammatory
358 response(*123,124*). Such activation has been implicated in modulating the activity of
359 cortical networks(*125*). Studies suggest that opioid dependence induces shifts in the
360 states of network connectivity in cortical and striatal circuits(*126*). Importantly, we
361 speculate interferon-γ signaling alters circuit activity, providing a mechanism for the
362 disturbances in circuit connectivity produced by opioids. Though still controversial, there
363 is growing evidence that opioids can also induce a neuroinflammatory response via direct
364 activation of TLR4 (toll-like receptor 4), a transmembrane receptor which activates NFκB
365 signaling and inflammatory cascades(*127*). Alternatively, independent of opioid action,
366 TLR4 may elicit an inflammatory response during opioid withdrawal(*128*). On the basis of

367 this evidence, we propose that disrupted network connectivity in the DLPFC as a
368 consequence of opioid-induced inflammatory responses drives changes in behaviors
369 associated with dependence, including craving and impaired decision making.

370 An effective neuroinflammatory response involves the interplay between immune
371 cell activation and local ECM remodeling. The ECM is an assembly of adhesion
372 molecules, proteins, polysaccharides, and proteoglycans, critical for BBB integrity(*129*),
373 along with cell proliferation, differentiation, and migration(*130*). Increasingly, ECM
374 remodeling is also implicated in synaptic plasticity(*131*). Importantly, the cytokines we
375 identified in DLPFC and NAc of OUD subjects, such as interferons and TNFs, modulate
376 ECM remodeling(*132,133*), and therefore, directly link neuroinflammation, ECM, and
377 opioids.

378 Both the formation and degradation of ECM in the brain depend on the aggregation
379 of a specific family of proteoglycans, chondroitin sulfate glycoaminoglycans (CS-
380 GAGs)(*134*). Significantly, CS-GAGs constitute the top shared pathway enriched
381 between DLPFC and NAc in OUD subjects. CS-GAGs aggregate in the perisynaptic
382 space in response to inflammation. This aggregation of CS-GAGs alters ECM structure
383 in the brain(*135*). These ECM structural changes consequently impact neurite outgrowth,
384 dendritic spine formation and morphology(*134,136*), and myelination(*137,138*). Indeed,
385 reduced myelination has been found in clinical neuroimaging and postmortem brain
386 studies of chronic opioid users(*139-143*), as well as in rodent models of chronic opioid
387 exposure(*144,145*). We therefore posit that opioid-induced changes in CS-GAG signaling
388 driven by neuroinflammation disrupt ECM structure and have profound consequences on
389 dendritic and synaptic plasticity. Consistent with this, preclinical opioid studies implicate

390 structural changes to the ECM with accompanying changes to dendritic and synaptic
391 plasticity(*135,146*). For example, ECM reorganization in the NAc via matrix
392 metalloproteinases (MMPs), which facilitate matrix degradation and reassembly, is
393 associated with increases in glutamatergic synaptic potentiation(*147*) and opioid relapse
394 behaviors(*135*). Importantly, our analyses identified a critical new hub linking ECM
395 remodeling via MMPs, neuroinflammation, and OUD. We found *TIMP1* as an OUD-
396 specific hub gene in the NAc, which is activated by pro-inflammatory cytokines that inhibit
397 MMPs[135]. Similarly, we discovered an additional OUD-specific hub gene, *TLR2*, which
398 also acts on MMPs to functionally reorganize excitatory synapses(*147*). We therefore
399 speculate: 1) opioid use elicits release of pro-inflammatory cytokines in the brain that
400 activate TIMP1 and TLR2, protein modulators of ECM organization(*148*); 2) these
401 activated modulators modify MMP activity to alter ECM organization; and 3) these
402 disturbances to ECM remodeling alter synaptic plasticity[136] and result in the behavioral
403 changes related to OUD. Future experiments will directly test these possibilities.

404 The primary resident immune cells in the brain are microglia. In response to
405 inflammation, microglia are locally recruited and activated, causing these cells to release
406 cytokines. Under normal physiological circumstances, microglia serve a neuroprotective
407 role. However, in response to prolonged activation, microglia transition to a reactive state,
408 which results in the uncontrolled release of pro-inflammatory cytokines. This ultimately
409 leads to neurotoxicity and further potentiates local damage.

410 Multiple lines of evidence point to the centrality of microglia in the pathways we
411 have identified in OUD. First, microglial markers were significantly enriched across
412 DLPFC and NAc in subjects with OUD. Moreover, our cell-type marker-based approach

413 revealed that the top differentially expressed transcript, *HSD17B14*, was highly correlated
414 with microglial markers. This gene encodes an enzyme that responds to both pro- and
415 anti-inflammatory cytokines to maintain microglial homeostasis during acute
416 inflammation(*74*). Second, our cell-type marker analysis revealed pathways involved in
417 microglial activation as well as the activation of additional immune cell types, including
418 $CD4^+$ and $CD8^+$ T-cells. Earlier work showed an interplay between microglia and $CD4^+$ T-
419 cells that was critical for neurodegeneration(*149*). This supports the possibility of
420 synergistic relationships between microglia and T-cells in potentiating neuroinflammation
421 in OUD. Third, the cytokines we have discussed above, including IL-1β, IL-6, IL-2, and
422 TNFα, are all secreted by activated microglia(*150*). These microglial associated cytokines
423 have been strongly implicated as modulators of opioid dependence-related
424 behaviors(*105,151,152*). Fourth, pathways identified in both DLPFC and NAc in OUD
425 map onto downstream signaling pathways associated with transcriptional regulation in
426 microglia in response to cytokine activation during inflammation. Specifically, our
427 transcriptional network analyses predicted the following top upstream regulators as
428 PPARγ, NFκB1, RELA, STAT1, and SP1. While microglia rely on multiple families of
429 transcription factors(*153*), our findings in OUD largely identify signal dependent
430 transcription factors that are important for guiding microglial response to inflammatory
431 signals. For example, PPARγ is a nuclear transcription factor preferentially expressed in
432 human microglia. PPARγ is activated in response to neuroinflammation and leads to anti-
433 inflammatory responses that are neuroprotective(*153*). Additionally, NFκB1 and RELA
434 form a complex in response to inflammatory stimuli, initiating a cascade of signaling well-
435 established in mediating cellular responses to injury and inflammation(*108,109*). Aberrant

436 activation of STAT1 in microglia leads to the transcription of several pro-inflammatory
437 cytokines. Intriguingly, STAT1-dependent signaling regulates the expression of the
438 human μ-opioid receptor via IL-6, another pro-inflammatory cytokine that we identified in
439 our analyses(*154*). Finally, we identified two pathways that are intimately linked to
440 microglial responses to inflammation: ameboidal migration and integrin signaling.
441 Integrins tether microglia to neurons by linking these cell types to the ECM scaffold(*155*).
442 Microglia rely on the ECM for ameboidal migration, further linking microglia, ECM, and
443 neuroinflammation in OUD.

444 In addition to changes in protein-coding transcripts, we discovered that subjects
445 with OUD also exhibited marked changes in lncRNAs compared to controls. LncRNAs
446 are key regulators of gene and protein expression via transcriptional, post-transcriptional,
447 translational and post-translational regulation(*156*). Several of the lncRNAs we identified
448 in OUD subjects, *AC0101086.3, BAALC.AS1,* and *AL136366.1*, are implicated in both
449 neurotransmission and neuroinflammation. In DLPFC, we found *AC0101086.3* to be an
450 OUD-specific hub lncRNA. This lncRNA is located proximally to *CLEC2D*, which encodes
451 ELT1, the functional ligand for the natural-killer cell receptor NKR-P1A. NKR-P1A controls
452 immunosurveillance via natural-killer, dendritic, and B-cells(*87,88*). In NAc, we found
453 *BAALC.AS1* and *AL136366.1* as OUD-specific hub lncRNAs. *BAALC* is involved in lipid
454 raft formation and membrane plasticity in neurons. This lncRNA has also been associated
455 with intellectual ability(*157*) and late-onset Alzheimer's Disease(*158*). *AL136366.1*
456 interacts with the transcription factor NFIB, involved in brain development(*159,160*),
457 intellectual disability(*161*), and astrocyte proliferation(*162,163*).

458 Functional alterations at the circuit-level occur across multiple brain regions in
459 opioid dependence(*3*) and during treatment response(*164*). One such change occurs at
460 the transcriptional level, where different brain regions can increasingly synchronize their
461 patterns of transcription. There is evidence that increases in transcriptional synchrony
462 across brain regions occur in response to insults including stress and drugs of
463 abuse(*165,166*). Consistent with this, we found significant transcriptional synchrony
464 between DLPFC and NAc in OUD subjects. To date, the precise relevance of such
465 profound synchrony remains unclear. We speculate that, because the ranking, effect size,
466 and direction of change in numerous transcripts is highly similar between brain regions,
467 such synchrony may represent a common pathophysiological response to
468 neuroinflammation in OUD. Clearly, further work is required to explore this possibility.

469 Integrating large-scale gene expression profiles with relevant GWAS findings
470 reveals novel gene-trait associations in OUD. We demonstrated that downregulated
471 genes in the NAc of OUD subjects were significantly enriched for GWAS of risky
472 behavior(*93*). Risky behavior forms a functional triad with mood and impulsivity(*167*),
473 where impulsivity is a risk factor for substance dependence including OUD(*168-170*). Our
474 findings therefore support relationships between genetic risk, brain region-specific
475 transcriptional changes, and vulnerability to OUD.

476 Overall, our data reveal new connections between the brain's immune system and
477 opioid dependence in the human brain. These results provide a novel putative mechanism
478 across transcriptional networks, biological pathways, and specific cell types for the
479 detrimental neuroadaptations across corticostriatal circuitry that result from chronic

480 opioids and OUD. The insights provided by our work offer the opportunity for new
481 therapeutic targets with improved efficacy to treat OUD.

482

483 **Materials and Methods**

484 *Human Subjects*

485 Brain specimens (n=40) were obtained during routine autopsies conducted at the
486 Office of the Allegheny County of the Medical Examiner (Pittsburgh, PA) after consent
487 was obtained from the next-of-kin. An independent committee of clinicians made
488 consensus, lifetime DSM-IV diagnoses for each subject using the results of a
489 psychological autopsy, including structured interviews with family members and review of
490 medical records, as well as toxicological and neuropathological reports(*171*). The same
491 approach was used to confirm the absence of lifetime psychiatric and neurologic clinical
492 disorders in the unaffected comparison subjects (controls). All procedures were approved
493 by the University of Pittsburgh Committee for Oversight of Research and Clinical Training
494 Involving Decedents and Institutional Review Board for Biomedical Research.

495 In order to control for experimental variance and to reduce biological variance
496 between diagnostic groups, each subject meeting diagnostic criteria for opioid
497 dependence at time of death (n=20) was matched with one control subject (n=20)
498 perfectly for sex and as closely as possible for age (Table 1). Subject groups did not differ
499 in mean age, postmortem interval (PMI), RNA integrity number (RIN), or tissue storage
500 time at -80°C (all t_{38}<1.18, all p>0.25). Brain pH significantly differed between diagnostic
501 groups (t_{38}=2.54, p=0.015); however, the mean difference was 0.2 pH units and of

502 uncertain biological significance. Subject groups significantly differed in racial
503 composition (χ^2=5.63, p=0.018). Demographic details on individual subjects are
504 presented in Table S1.

505

506 *RNA Sequencing*

507 The DLPFC (area 9) and NAc were identified from fresh-frozen right hemisphere
508 coronal tissue blocks using anatomical landmarks(*172*), and ~50mg of tissue was
509 collected via cryostat for each subject in a manner that minimizes contamination from
510 white matter and other striatal subregions and ensures excellent RNA
511 preservation(*173,174*). Tissue was homogenized in TRIzol (Invitrogen, Carlsbad, CA)
512 and RNA extracted using the RNeasy Lipid Tissue Mini Kit (Qiagen). RNA integrity was
513 assessed using a Bioanalyzer (Agilent) and concentration was determined using a Qubit
514 fluorometer (Invitrogen). Libraries were constructed using TruSeq Total RNA sample kit
515 and sequenced by Illumina NextSeq 500. All samples were sequenced across all lanes
516 to avoid lane bias by a technician blind to treatment groups (paired-end 75 cycles).
517 Average sample coverage was 29 million reads before alignment. FastQC was used to
518 assess the quality of the data. Per base sequence quality was high (mean Phred>30),
519 indicating good quality of the experimental data. HISAT2 was used to align the read to
520 the Ensembl human reference genome (GRCh38.p13) reference(*175*). The resulting bam
521 files after alignment were converted to expression count data using HTSeq(*176*). The
522 RNAseq count data were transformed to log*2* count data using voom function of the
523 Bioconductor limma package(*177,178*). A total of 80 samples (20 control DLPFC, 20
524 control NAc, 20 OUD DLPFC, 20 OUD NAc) with 60,676 genes preprocessed together.

525 Low expression genes were filtered out and 15,042 genes remained (retained genes with
526 log_2 transformed counts per million greater than 1 in 50% or more subjects).

527

528 *Differential expression*

529 Differential expression was assessed using limma with covariate selection, as
530 previously(*179*). Briefly, for each gene, we first adjusted the difference of expression
531 (log_2FC) with covariates (sex, age, race, PMI, pH, RIN) by including each covariate in the
532 regression model. Next, at most 2 covariates were selected to be included in the full model
533 using Bayesian information criterion (BIC) for each gene individually(*180*). We report
534 corrected p-values and Benjamini-Hochberg q-values (*181*). Genes with corrected $p<0.01$
535 and $log_2FC>0.26$ were considered differentially expressed(*166,182,183*). For each brain
536 region, the top 250 DE genes were ordered by log_2FC and used for unsupervised
537 clustering of subjects. Biotypes of detected genes were determined using metaseqR
538 (v3.11)(*184*). Overrepresentation of pathway and gene ontology (GO) categories was
539 assessed using Metascape (http://www.metascape.org), with expressed genes as
540 background. We assessed enrichment using GO, KEGG, Hallmark, Canonical Pathways,
541 Reactome, BioCarta, and CORUM. Pathway enrichment was performed for each brain
542 region separately and for the list of DE genes that were shared across brain regions.

543

544 *Determination of differential expression upstream regulators*

545 INGENUITY® Pathway Analysis (Qiagen) was used to determine predicted
546 upstream regulators of DE genes with expressed genes as background considering direct

547 and indirect relationships. As a complementary approach, we used HOMER (v4.11) to
548 predict upstream factors that might drive differential expression patterns(*25*). HOMER
549 determines if binding motifs within a gene set are enriched compared to what is expected
550 in the background gene list; all promoters (except those chosen for analysis) were used
551 as background.

552

553 *Chromatin states of differentially expressed genes*

554 Chromatin states from the 15-state model trained on histone modifications were
555 obtained from the Roadmap Epigenomics Project(*72*). Genome state annotations were
556 converted to hg38 from hg19(*185*). ENSEMBL genes (v79) were matched to chromatin
557 states based on the annotated transcription start site(*186*). Gene expression differences
558 measured in the DLPFC in OUD subjects compared to control subjects were compared
559 to PFC chromatin states. No chromatin states were available for the NAc, so chromatin
560 states for the anterior caudate were used as a substitute, as both regions are dominated
561 by medium spiny neurons. The hypergeometric test was used to calculate the enrichment
562 of observed overlaps in the OUD-higher and OUD-lower gene sets of both brain regions
563 to each chromatin state in corresponding brain region.

564

565 *Identification of OUD-specific co-expression networks*

566 In each brain region separately, we used weighted gene co-expression network
567 analysis (WGCNA) to identify gene modules with similar expression patterns across
568 samples(*187,188*). WGCNA was performed using the 5000 most variable genes across

569 samples. Modules were built using OUD samples and module preservation analysis was
570 performed to determine robustness of modules(*189*). Module differential connectivity
571 (MDC) was used to quantify differences in co-expression between OUD and control
572 samples; MDC is the ratio of the connectivity of all gene pairs in a module from OUD
573 subjects to that of the same gene pairs from control subjects(*190*). MDC >1 indicates gain
574 of connectivity, while MDC <1 indicates loss of connectivity. To statistically test the
575 significance of MDC, we estimated the p-value based on two types of shuffling schemes:
576 1) shuffled samples – adjacent matrix with non-random nodes but random connections;
577 2) shuffled genes – adjacent matrix with random nodes but non-random connections.
578 Data were permuted 1000 times. P-values were converted to q-values following
579 Benjamini Hochberg procedure, and MDC q<0.05 was considered significant.

580

581 *Module enrichment*

582 We used Fisher's exact test to determine whether DE genes were enriched within
583 WGCNA modules. Overrepresentation of pathway and gene ontology (GO) categories for
584 each module was assessed using Metascape (http://www.metascape.org), with the 5000
585 WGNCA-analyzed genes as background. We assessed enrichment using GO, KEGG,
586 Hallmark, Canonical Pathways, Reactome, BioCarta, and CORUM. To examine overlap
587 of pathways, pathways are hierarchically clustered into a tree based on Kappa-statistical
588 similarities among gene memberships (0.3 Kappa score used as threshold to cast tree
589 into term clusters and thickness of edge represents similarity score). A subset of
590 representative terms from this cluster were selected for network layout, where each term
591 is represented by a circle node (size proportional to number of input genes within term

592 and color intensity reflects p-value). The network is visualized with Cytoscape using
593 Community cluster with categorical labels representing multiple clusters.

594

595 *Identification of module network structure*

596 ARACNe was used to identify hub and OUD-specific hub genes for network
597 analysis(*191*). A gene is considered a hub if the N-hob neighborhood nodes (NHNN) is
598 significantly higher than the average NHNN. A hub gene is considered an OUD-specific
599 hub if it attains hub status in OUD, but not control subjects. Cytoscape 3.8.0 was used to
600 generate networks of hub genes; only correlations >0.98 are included in the networks.
601 Overlap of pathways within brain region was assessed using Metascape and Cytoscape
602 (Community Cluster, GLay).

603

604 *Determination of overlapping patterns between DLPFC and NAc*

605 We first determined overlap between DE patterns between the DLPFC and NAc
606 using strict cutoffs, in which genes needed to have p<0.01 across both brain regions. We
607 also used rank rank hypergeometric overlap (RRHO) as a threshold-free method to
608 evaluate the overlap of differential expression patterns between the DLPFC and
609 NAc(*192,193*). RRHO identifies overlap between two ranked lists of differential gene
610 expression. For each of the two datasets, RRHO ranks the entire gene list by DE p-value
611 and effect size direction; one dataset is represented on the X-axis and one on the Y-axis.

612

613 *Cell-type-specific differential expression analysis*

614 We estimated cell-type fractions from bulk RNA-seq data using Digital Sorting
615 Algorithm (DSA)(*194*), a marker-guided deconvolution method. The bulk data are
616 deconvolved in BRETIGEA into six cell types: astrocytes, endothelial cells, microglia,
617 neurons, oligodendrocytes, and OPC(*195*). OUD and control subjects are compared for
618 enrichment of each cell type using hypergeometric t-tests adjusting for brain region. We
619 then conducted cell-type-specific (CTS) differential expression analysis with CellDMC for
620 each brain region(*73*). CellDMC is designed for detecting CTS differentially methylated
621 sites but is also applicable to gene expression data. Significant genes are defined as a
622 false discovery rate (FDR)<0.05.

623

624 *Relationship of identified DE lists to GWAS*

625 We separated DLPFC and NAc up and down regulated genes in OUD by the sign
626 of their $\log_2$FC values. Region-specific differentially up- and down-regulated genes with a
627 corrected p<0.01 was used to construct the foregrounds for GWAS enrichment. We
628 selected intronic and intergenic regions of a marker gene from the GENCODE human
629 hg38 comprehensive gene annotation release 33. For each set of gene markers, we took
630 the region spanning the gene body and subtracted exons to define introns. Then, we took
631 the 20kb regions flanking the gene body as the proximal intergenic regions. To avoid
632 collision with nearby genes in dense, gene-rich loci, we removed flanking sequences that
633 overlap exons. We then merged intronic and intergenic regions for each brain region and
634 $\log_2$FC gene set foreground. We found in our hands that the LD score (LDSC) GWAS
635 enrichment analysis is sensitive to selected background set of matched regions for proper
636 enrichment above the foreground set. We combined intronic and flanking intergenic

637 regions as above for all hg38 genes from the GENCODE annotation to create the
638 background for LDSC GWAS enrichment analysis.

639 We computed the partitioned heritability (GWAS enrichment) of brain region-
640 specific noncoding regions containing and surrounding up and down regulated OUD gene
641 marker sets (corrected $p<0.01$) for addiction-related variants using the LD score
642 regression pipeline for cell type-specific enrichment as outlined in
643 https://github.com/bulik/ldsc/wiki(*196,197*). The traits of brain-related GWAS include
644 multisite chronic pain(*198*), tendency to engage in risky behavior(*93*), schizophrenia
645 risk(*199*), opioid dependence(*200*), cannabis use(*201*), diagnosis of obsessive-
646 compulsive disorder (*202*), age of smoking initiation(*94*), heaviness of smoking(*94*),
647 alcoholic drinks per week(*94*), having ever regularly smoked(*94*), current versus former
648 smokers(*94*), highest level of educational attainment(*157*), sleep duration(*203*). The traits
649 of the non-brain related traits include lean body mass(*204*), bone mineral density(*205*),
650 and coronary artery disease(*206*). The pipeline produced LD score regression coefficient,
651 coefficient error, and coefficient p-value estimates. The p-values of the LD score
652 regression coefficients were adjusted for false discovery rate (α=0.1) on GWAS
653 enrichments performed on all GWAS for foregrounds at one p-value cutoff since genes
654 are shared in foregrounds of less stringent cutoffs. A significant p-value indicates
655 enrichment of the foreground genomic regions for GWAS SNPs relative to the
656 background.
657

Figure Legends

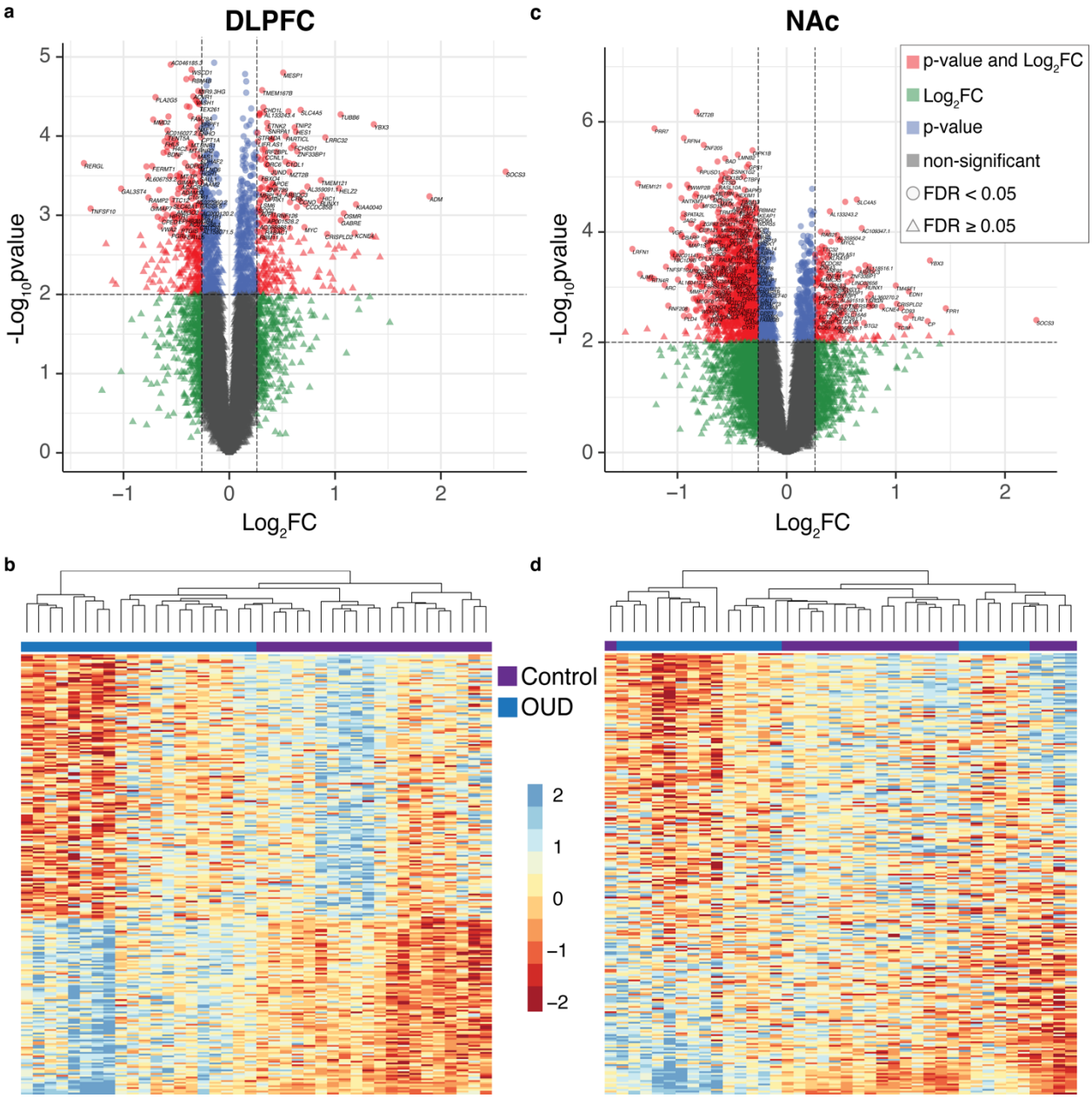

Fig. 1. Transcriptomic changes in DLPFC and NAc from OUD subjects. (a) Log_2FC plotted relative to $-log_{10}$p-value by volcano plot for DE genes in DLFPC. Horizontal dashed lines represent p-value significance cutoff of corrected $p<0.01$, while vertical dashed lines represent log_2FC cutoffs of $\leq$-0.26 or $\geq$0.26 (FC$\geq$1.2). Red circles represent DE genes

664 that reach significance, log_2FC, and FDR<0.05 cutoffs. **(b)** Heatmap of the top 250 DE
665 genes (corrected p<0.01 and log_2FC of ≤-0.26 or ≥0.26) clustered by gene and subject.
666 Each column represents a subject (controls, purple; OUD, blue). Subjects within groups
667 cluster together. **(c)** Volcano plot for DE genes in NAc. Note the large numbers of genes
668 that are significantly reduced in expression compared to genes that are increased. **(d)**
669 Heatmap of the top 250 DE genes clustered by gene and subject. Overall, subjects within
670 groups cluster together with several groups of subjects forming separate clusters.

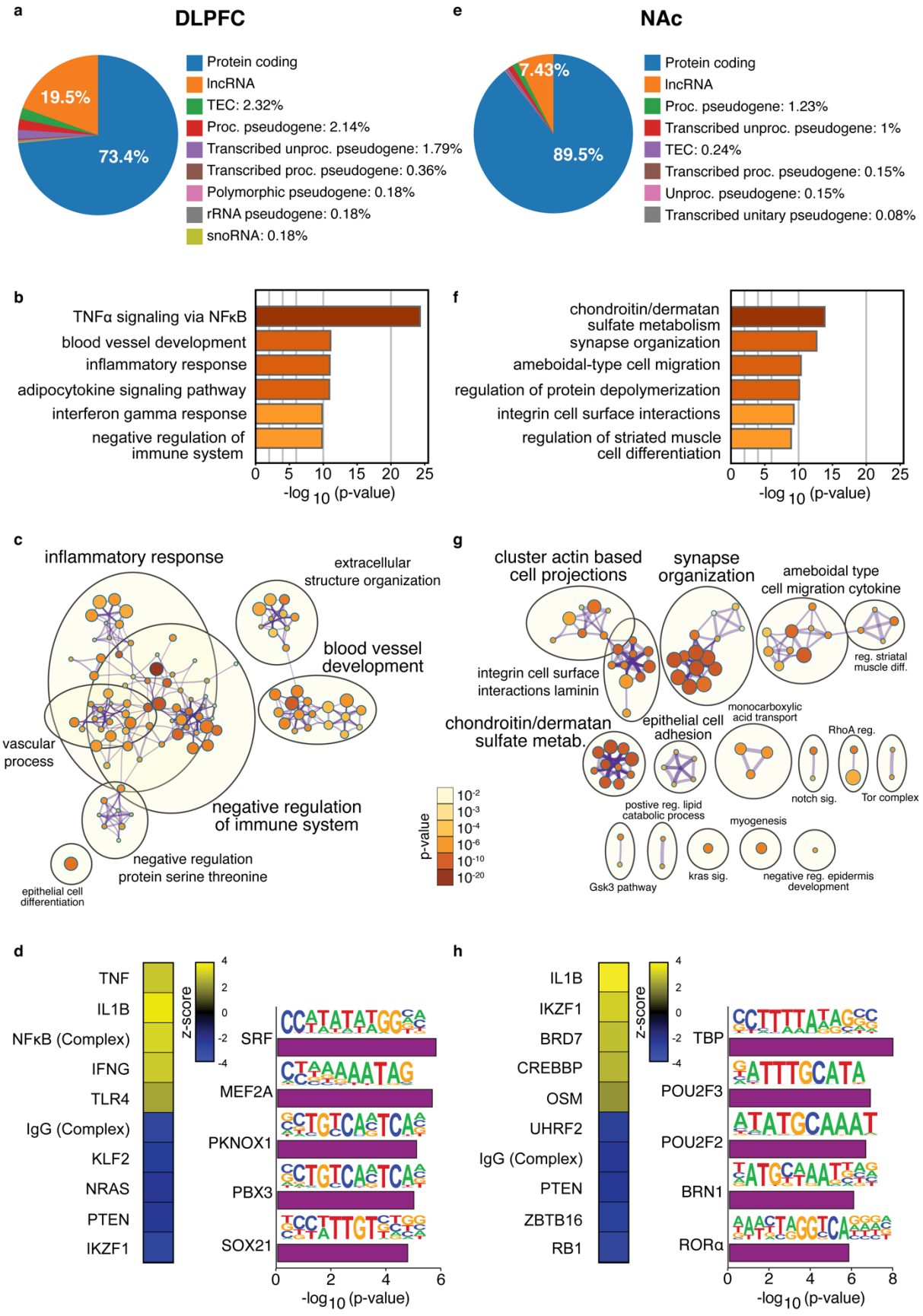
a
DLPFC
19.5%
73.4%
Protein coding
lncRNA
TEC: 2.32%
Proc. pseudogene: 2.14%
Transcribed unproc. pseudogene: 1.79%
Transcribed proc. pseudogene: 0.36%
Polymorphic pseudogene: 0.18%
rRNA pseudogene: 0.18%
snoRNA: 0.18%
e
NAc
7.43%
89.5%
Protein coding
lncRNA
Proc. pseudogene: 1.23%
Transcribed unproc. pseudogene: 1%
TEC: 0.24%
Transcribed proc. pseudogene: 0.15%
Unproc. pseudogene: 0.15%
Transcribed unitary pseudogene: 0.08%
b
TNFα signaling via NFκB
blood vessel development
inflammatory response
adipocytokine signaling pathway
interferon gamma response
negative regulation of immune system
0 5 10 15 20 25
-log 10 (p-value)
f
chondroitin/dermatan sulfate metabolism
synapse organization
ameboidal-type cell migration
regulation of protein depolymerization
integrin cell surface interactions
regulation of striated muscle cell differentiation
0 5 10 15 20 25
-log 10 (p-value)
c
inflammatory response
extracellular structure organization
blood vessel development
vascular process
negative regulation of immune system
negative regulation protein serine threonine
epithelial cell differentiation
g
cluster actin based cell projections
synapse organization
ameboidal type cell migration cytokine
reg. striatal muscle diff.
integrin cell surface interactions laminin
chondroitin/dermatan sulfate metab.
epithelial cell adhesion
monocarboxylic acid transport
RhoA reg.
notch sig.
Tor complex
postive reg. lipid catabolic process
myogenesis
Gsk3 pathway
kras sig.
negative reg. epidermis development
p-value
10-2
10-3
10-4
10-6
10-10
10-20
d
TNF
IL1B
NFκB (Complex)
IFNG
TLR4
IgG (Complex)
KLF2
NRAS
PTEN
IKZF1
z-score
4 2 0 -2 -4
SRF
MEF2A
PKNOX1
PBX3
SOX21
0 2 4 6
-log10 (p-value)
h
IL1B
IKZF1
BRD7
CREBBP
OSM
UHRF2
IgG (Complex)
PTEN
ZBTB16
RB1
z-score
4 2 0 -2 -4
TBP
POU2F3
POU2F2
BRN1
RORα
0 2 4 6 8
-log10 (p-value)

671

672 **Fig. 2**. **Differential enrichment of transcriptional pathways between DLPFC and NAc**
673 **in OUD subjects. (a)** Biotypes of DE genes (corrected $p<0.01$ and $\log_2FC$ of $\leq$-0.26 or
674 $\geq$0.26) in DLPFC. Protein coding genes represent the majority of DE genes (blue; 73.4%)
675 followed by lncRNAs (orange; 19.5%). **(b)** Pathways enriched from DE genes in DLPFC
676 mainly include pathways related to inflammation and immune function. **(c)** Significantly
677 enriched terms based on pathways included in multiple annotated sets (*e.g.,* GO, KEGG,
678 hallmark, etc.) using hypergeometric p-values and enrichment factors. Note inflammatory
679 response and immune function represent majority of pathways, along with several non-
680 overlapping pathways involved in blood vessel development and vascular processes. **(d)**
681 IPA predicted upstream regulators known to be involved in immune function. Analysis
682 focused on regulators predicted to be significantly activated or inhibited (z-scores, yellow
683 to blue gradient represents activated or inhibited, respectively). Top predicted
684 transcription factors and promotor binding sequences by HOMER from DE genes in
685 DLPFC. Several of these transcription factors interact with TNF-dependent signaling,
686 including SRF, MEF2A, and PBX3. **(e)** Biotypes of DE genes in NAc. Protein coding
687 genes represent the majority of DE genes (blue; 89.5%) followed by lncRNAs (orange;
688 7.43%). **(f)** Pathways enriched in DE genes in NAc mainly include pathways related to
689 chondroitin and dermatan sulfate metabolism and synapse organization. **(g)** In the NAc,
690 pathways were distinct, with few overlapping nodes and biological categories. **(h)** IPA
691 predicted upstream regulators known to be involved in immune function (activated: IL1B,
692 OSM; inhibited: IgG complex), synaptic plasticity and myelination (inhibited: PTEN),
693 autophagy (inhibited: ZBTB16), and epigenetic regulation of transcription, including

694 chromatin remodeling (activated: BRD7, IKZF1, CREBBP; inhibited: RB1) and DNA

695 methylation (inhibited: UHRF2).

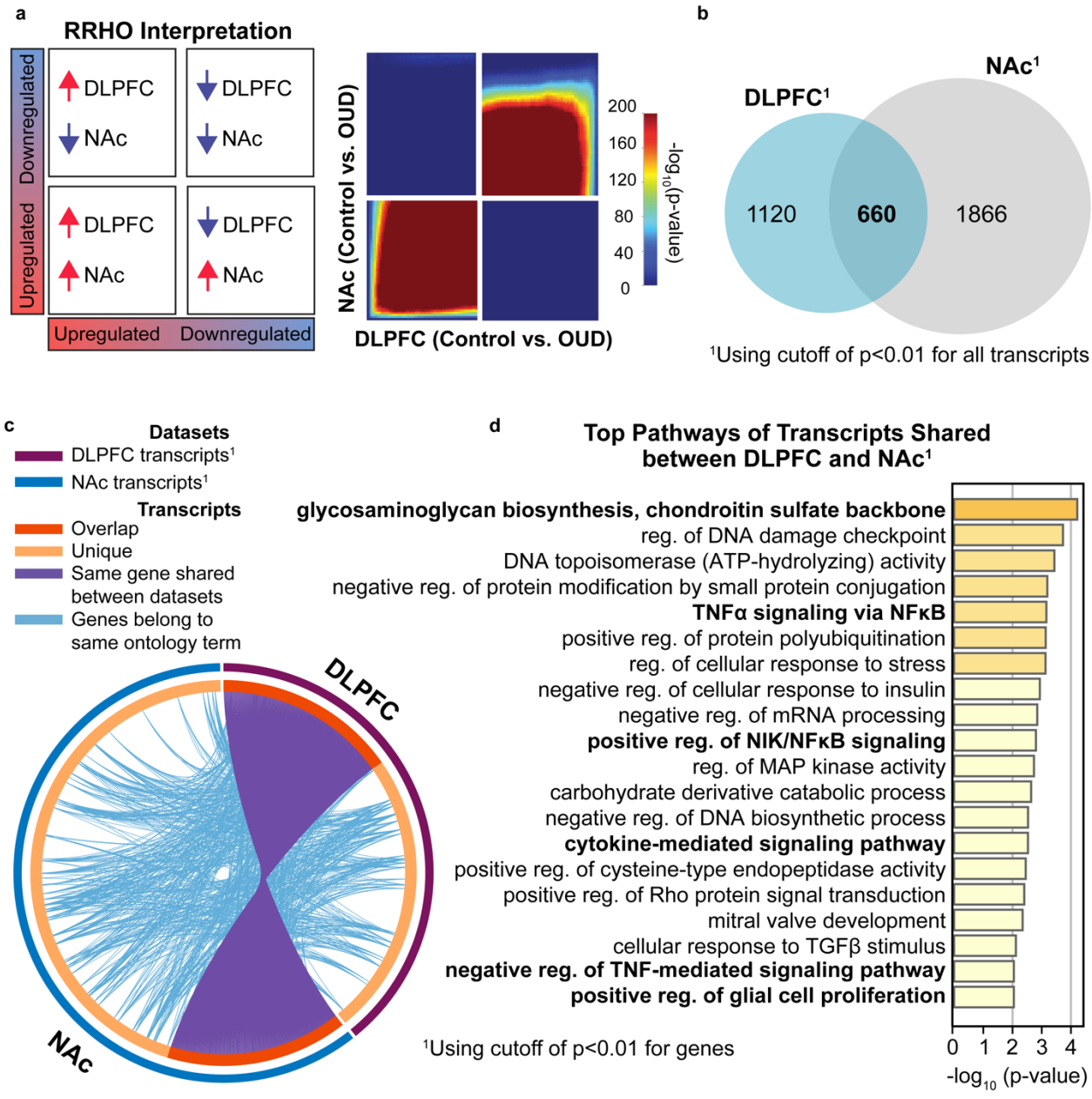

696

697 **Fig. 3. High transcriptional concordance reveals commonly altered molecular**

698 **pathways between brain regions associated with opioid dependence. (a)** RRHO plot

699 indicating high degree of overlap, or transcriptional concordance, between DLPFC and

NAc in OUD subjects. **(b)** Venn diagram of DE genes between DLPFC and NAc. **(c)** DE genes (purple lines) and their ontology (light blue lines) highly overlapped (orange) between DLPFC and NAc. **(d)** Top 20 pathways of DE genes shared between DLPFC and NAc. Many of these pathways are related to ECM and neuroinflammatory signaling.

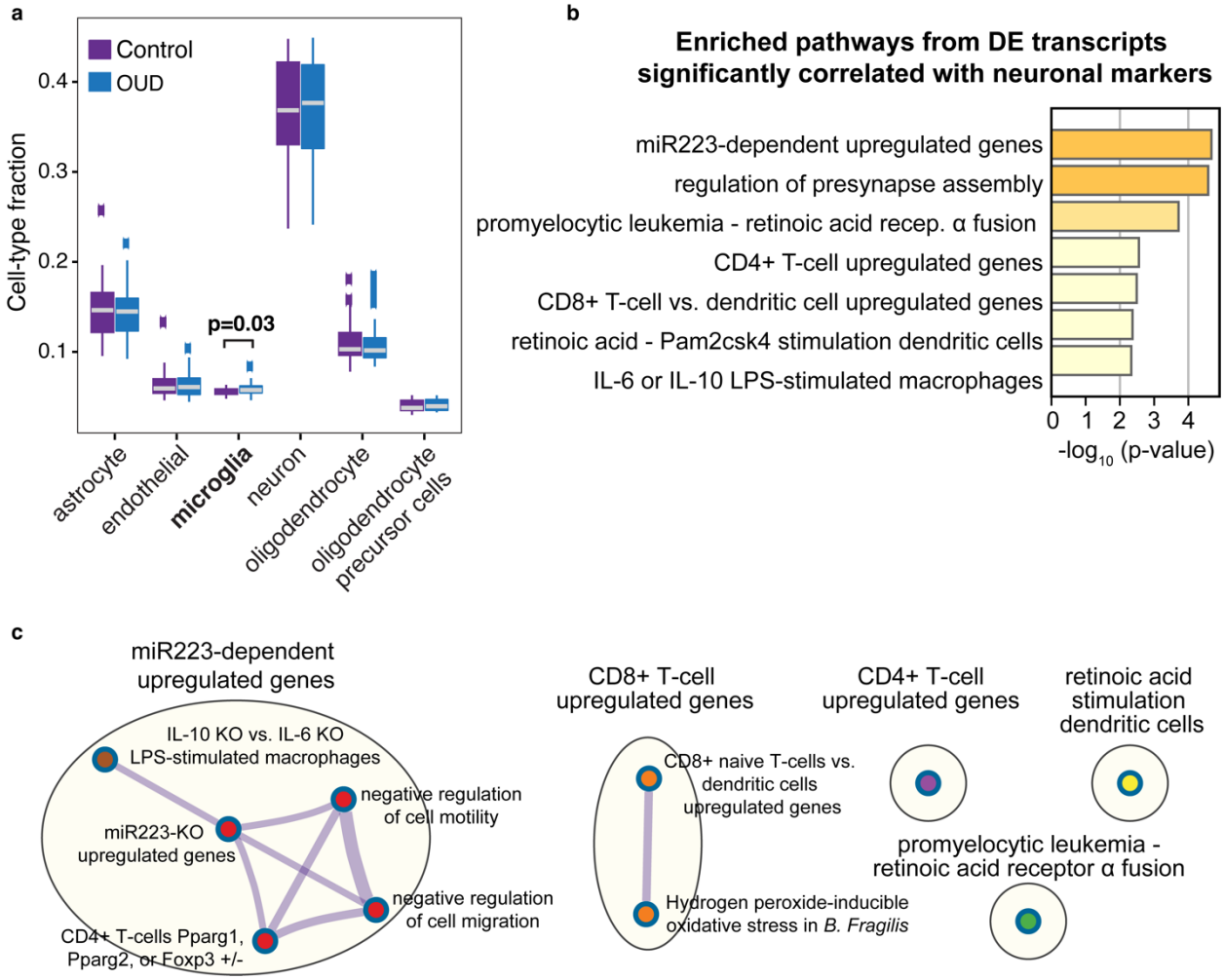

Fig. 4. Predicted microglial cell-type enrichment in both DLPFC and NAc. (a) Deconvolution analyses indicates modest enrichment of microglia gene markers in DLPFC and NAc of OUD subjects ($p<0.03$; hypergeometric t-test controlling for brain region), consistent with enrichment of pathways in DE genes related to immune function. **(b)** Pathway enrichment analysis on the significantly altered DE genes in neurons

710 identified pathways related to inflammation**. (c)** Significantly enriched terms based on
711 pathways included in multiple annotated sets (*e.g.,* GO, KEGG, hallmark, etc.) using
712 hypergeometric p-values and enrichment factors. The network is visualized with
713 Cytoscape using Community cluster with categorical labels representing multiple clusters.
714 Individual nodes are also labeled. Note nodes are related to presynaptic structure and
715 function and miR233-dependent regulation of macrophage and T-cell activation.

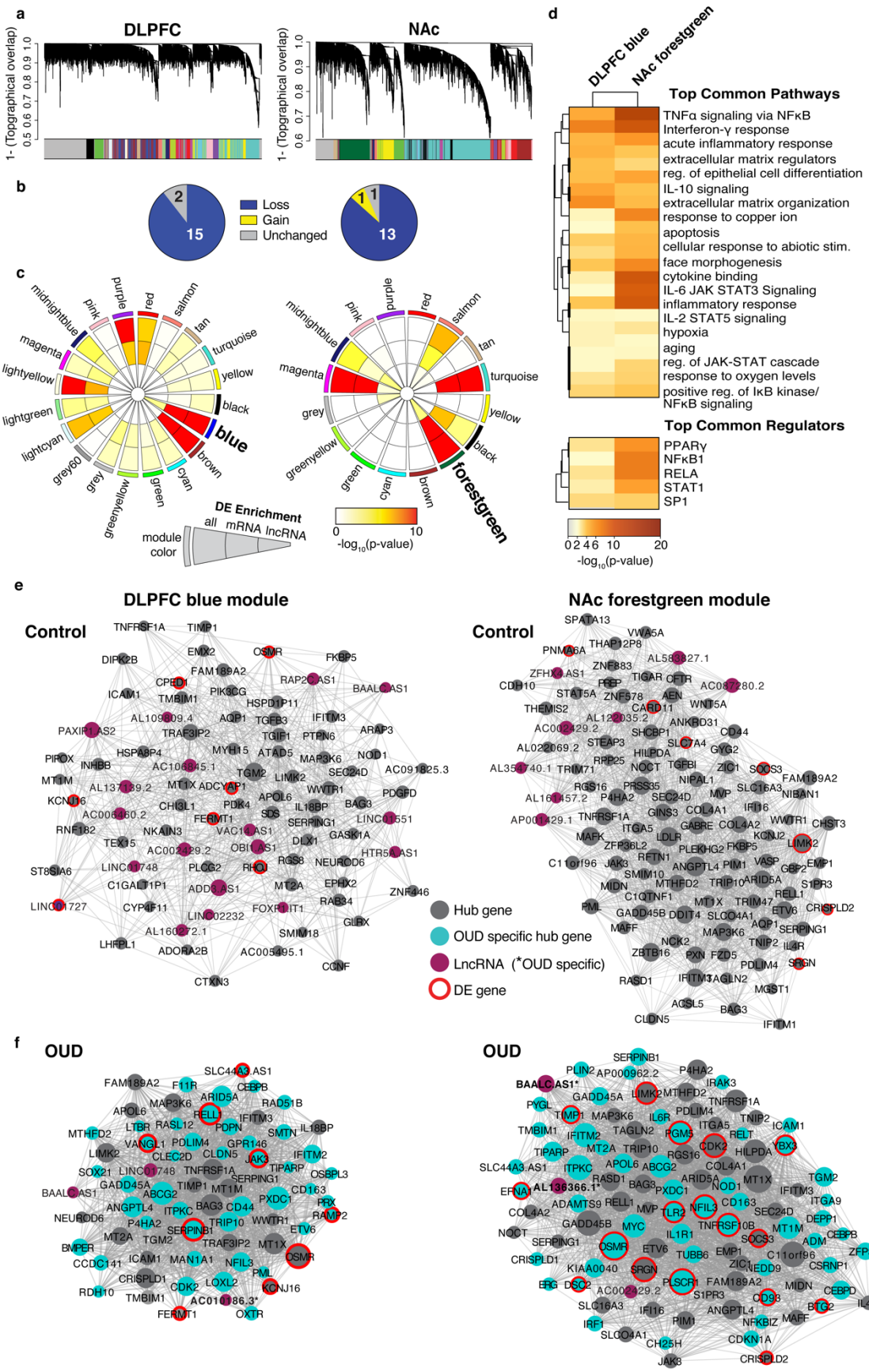
a
DLPFC
NAc
1- (Topgraphical overlap)
b
Loss
Gain
Unchanged
15
2
13
1
1
c
midnightblue
pink
purple
red
salmon
tan
turquoise
yellow
black
blue
brown
cyan
green
greenyellow
grey
grey60
lightcyan
lightgreen
lightyellow
magenta
forestgreen
DE Enrichment
all
mRNA
lncRNA
module color
-log10(p-value)
d
DLPFC blue
NAc forestgreen
Top Common Pathways
TNFα signaling via NFκB
Interferon-γ response
acute inflammatory response
extracellular matrix regulators
reg. of epithelial cell differentiation
IL-10 signaling
extracellular matrix organization
response to copper ion
apoptosis
cellular response to abiotic stim.
face morphogenesis
cytokine binding
IL-6 JAK STAT3 Signaling
inflammatory response
IL-2 STAT5 signaling
hypoxia
aging
reg. of JAK-STAT cascade
response to oxygen levels
positive reg. of IκB kinase/ NFκB signaling
Top Common Regulators
PPARγ
NFκB1
RELA
STAT1
SP1
-log10(p-value)
e
DLPFC blue module
Control
NAc forestgreen module
Control
Hub gene
OUD specific hub gene
LncRNA (*OUD specific)
DE gene
f
OUD
OUD

717 **Fig. 5. OUD associated gene networks in DLPFC and NAc. (a)** Weighted gene co-
718 expression network analysis (WGCNA) was used to generate co-expression modules,
719 with the network structure generated on each brain region separately. The identified
720 modules that survived module preservation analysis were arbitrarily assigned colors and
721 the dendrogram shows average linkage hierarchical clustering of genes. **(b)** Pie charts
722 summarize results from the module differential connectivity (MDC) analysis compared
723 OUD to control subjects. The majority of modules were lost in control subjects, revealing
724 OUD-specific modules in both DLPFC and NAc. **(c)** Circos plot identified by module
725 names and colors. Enrichment for full list of differentially expressed (DE) genes, protein-
726 coding (mRNA), and long non-coding RNAs (lncRNA), are indicated by semi-circle colors
727 within each module, with increasing warm colors indicating increasing $-\log_{10}$ p-value.
728 LncRNA enrichment was examined based on the high prevalence of these transcripts in
729 the Biotype analysis (see Figure 2a,e). MDC analysis indicated a loss of connectivity in
730 the DLPFC blue module and NAc forestgreen module. These modules were also enriched
731 for DE mRNA and lncRNAs. **(d)** Pathway enrichment analysis compared gene networks
732 within the DLPFC blue module and NAc forestgreen module. Warmer colors indicate
733 increasing $-\log_{10}$ p-value and highly shared pathways between the modules. Hub gene
734 co-expression networks of the DLPFC blue module **(e)** control subjects and (**f)** OUD
735 subjects, and networks of the forestgreen module in NAc **(e)** control subjects and **(f)** OUD
736 subjects. Node size indicates the degree of connectivity for that gene. Turquoise nodes
737 indicate OUD-specific hub genes, purple nodes indicate LncRNA gene, gray nodes
738 indicate hub genes, and red halos indicate DE genes. Edges indicate significant co-
739 expression between two particular genes.

740 **Tables**

741 **Table 1.** Subject summary demographic and tissue characteristics

Characteristic	Controls (n=20)	Opioid dependent (n=20)
Age	47.3 ± 9.5	46.9 ± 7.3
Sex	10M 10F	10M 10F
Race	13W 7B	19W 1B
PMI (hours)	15.7 ± 6.1	16.0 ± 5.3
Brain pH	6.6 ± 0.3	6.4 ± 0.2
RIN	8.0 ± 0.7	7.8 ± 0.7
Tissue Storage Time (months)	100.3 ± 86.1	103.0 ± 59.7

742 Values are mean ± SD. M, male; F, female; B, black; W, white

743

744 **Table 2.** Table reporting number of DE genes between OUD and control subjects for
745 DLPFC and NAc at various significance cutoffs. A permutation test was used to return
746 corrected p-values and Benjamini-Hochberg q-value are reported. Note the large
747 numbers of genes that are significantly changed in the NAc relative to the DLPFC from
748 OUD subjects.

	q < 0.01	**q < 0.05**	**q < 0.1**	**Corrected p < 0.01**	**Corrected p < 0.05**
DLPFC[1]	1 (1/0)	271 (108/163)	500 (203/297)	567 (228/339)	977 (413/564)
NAc[1]	53 (2/51)	1037 (150/887)	1572 (285/1287)	1305 (221/1084)	2095 (419/1676)

749 [1]Using cutoff of log2FC ≤ -0.26 and ≥ 0.26; (upregulated / downregulated)

750

751

752

753 **Supplementary Materials**

754 **Supplementary Materials and Methods**

755 *Relationship of identified DE lists to GWAS*

756 The summary statistics of GWAS SNPs used in these analyses were downloaded
757 and processed using the LDSC munge_sumstats function to filter rare or poorly imputed
758 SNPs. The HapMap SNPs excluding the MHC regions used to filter SNPs were
759 downloaded from http://ldsc.broadinstitute.org/static/media/w_hm3.noMHC.snplist.zip.
760 Column headings of each GWAS file were inspected to ensure the effect allele, non-effect
761 allele, sample size, p-value, and signed summary statistic for each SNP in each GWAS
762 were included and appropriate for the LDSC pipeline.

763 The LD scores were estimated for each foreground set and corresponding
764 background set with the LD score regression pipeline make_annot and ldsc functions
765 using hg38 1000 Genomes European Phase 3 (1000G EUR) cohort plink files
766 downloaded from https://data.broadinstitute.org/alkesgroup/LDSCORE/GRCh38/. The
767 baseline v1.2 files for cell type-specific enrichment in hg38 coordinates were downloaded
768 from the same link above and the corresponding weights `weights.hm3_noMHC' file
769 excluding the MHC region from https://data.broadinstitute.org/alkesgroup/LDSCORE/.
770 We find that HapMap SNPs and corresponding weights file used in the LDSC analyses
771 only referred to rsIDs, rather than genomic coordinates, so only the baseline and LD
772 statistics used to annotate the foreground and background files have to be in hg38
773 coordinates. An `enrichment.ldcts' file listing the annotated foreground/background pair
774 was created for each foreground. The partitioned heritability was estimated using the ldsc
775 function, which integrates the foreground and background LD score estimates, munged

776 GWAS SNP data, baseline variant data, and variants weights. The final function call to
777 GWAS enrichment is as follows:

```
778         python ldsc.py --h2-cts $Munged_GWAS \
779             --ref-ld-chr baseline_v1.2/baseline. \
780             --w-ld-chr weights.hm3_noMHC. \
781             --ref-ld-chr-cts enrichment.ldcts \
782             --out $Output_Label
```

a

	q < 0.01	q < 0.05	q < 0.1	Corrected p < 0.01	Corrected p < 0.05
DE[1]	0 (0/0)	0 (0/0)	0 (0/0)	97 (41/56)	509 (173/336)

[1]Using cutoff of $\log_2$FC ≤ -0.26 and ≥ 0.26; (higher DLPFC / higher NAc)

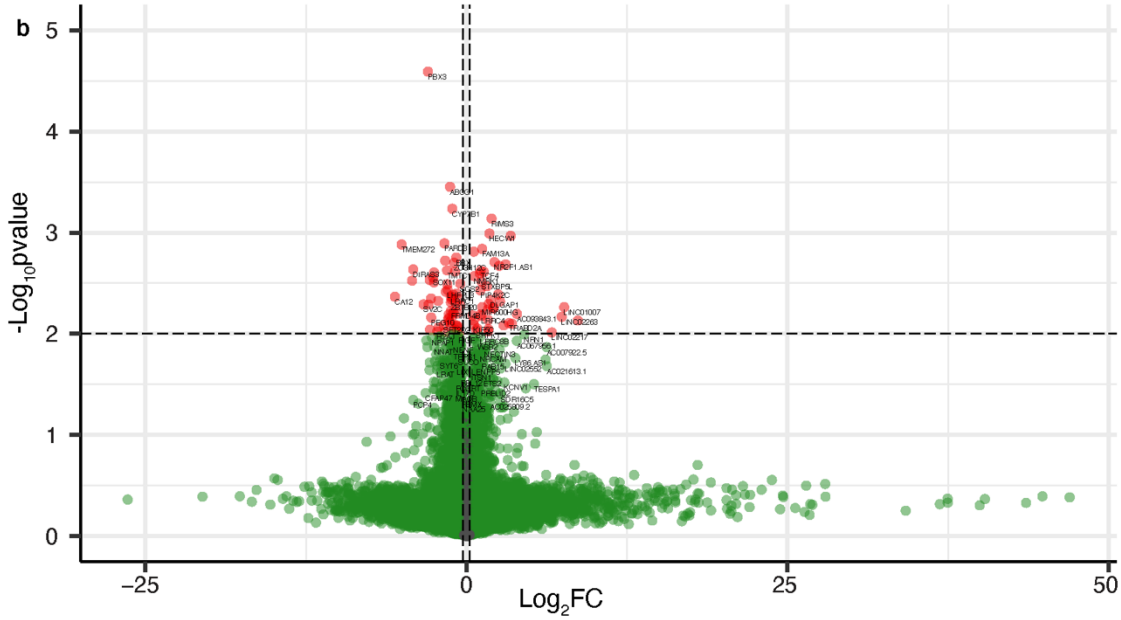

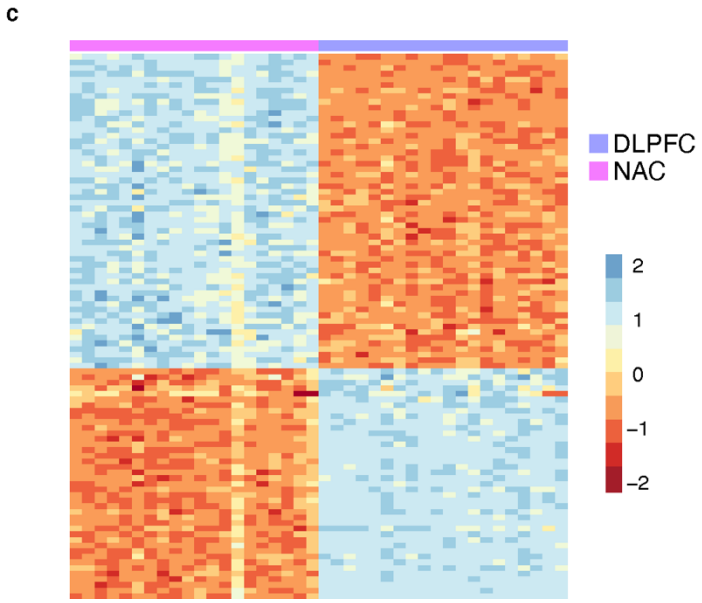

783

784 **Figure S1. Differentially expressed transcripts between DLPFC and NAc in control**
785 **subjects. (a)** Table reporting number of DE genes between the DLPFC and NAc of
786 control subjects at various significance cutoffs. A permutation test was used to return
787 corrected p-values and Benjamini-Hochberg q-value are reported**. (b)** Log_2FC plotted

relative to -$\log_{10}$p-value by volcano plot for DE genes in DLFPC compared to NAc. Horizontal dashed lines represent p-value significance cutoff of corrected p<0.01, while vertical dashed lines represent $\log_2$FC cutoffs of ≤-0.26 or ≥0.26 (FC≥1.2). Red circles represent DE genes that reach significance, $\log_2$FC, and FDR<0.05 cutoffs. **(c)** Heatmap of the top 250 DE genes (corrected p<0.01 and $\log_2$FC of ≤-0.26 or ≥0.26) clustered by gene. Each column represents a subject (controls, purple; OUD, blue).

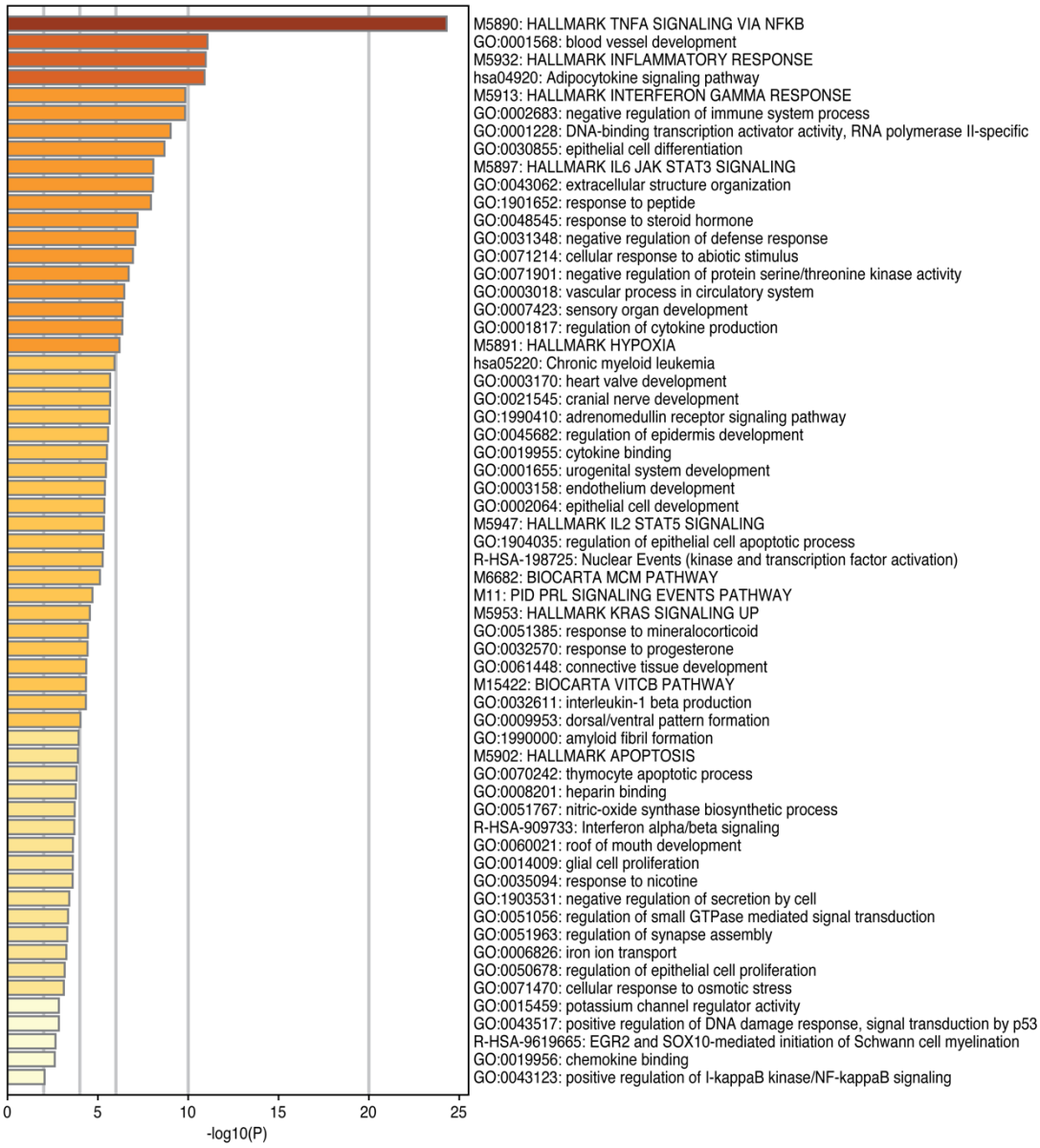

795 **Figure S2**. **Top pathways enriched from differentially expressed transcripts in the**

796 **DLPFC of OUD subjects.** All pathways significantly enriched in the DLPFC ranked by -

797 $\log_{10}$ p-value.

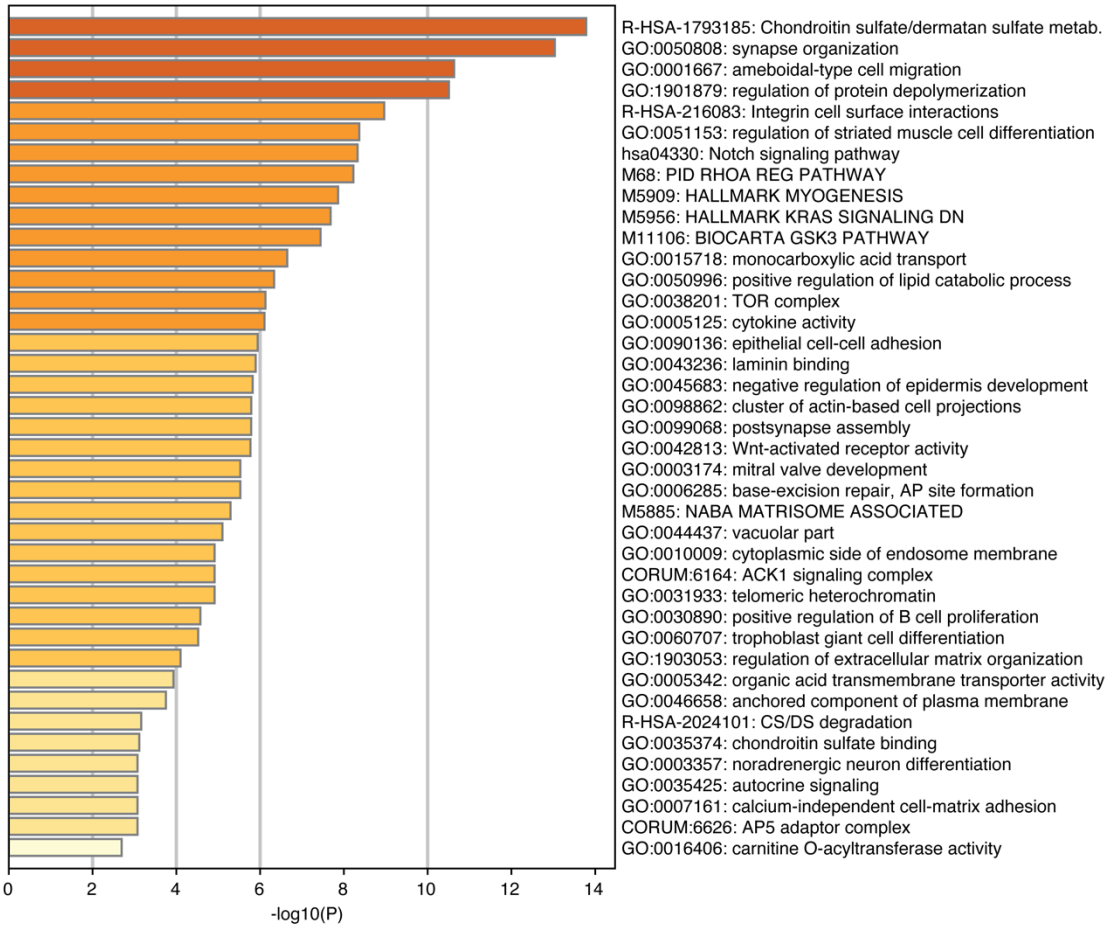

798

799 **Fig. S3. Top pathways enriched from differentially expressed genes in the NAc of**

800 **OUD subjects.** All pathways significantly enriched in the NAc ranked by -$\log_{10}$ p-value.

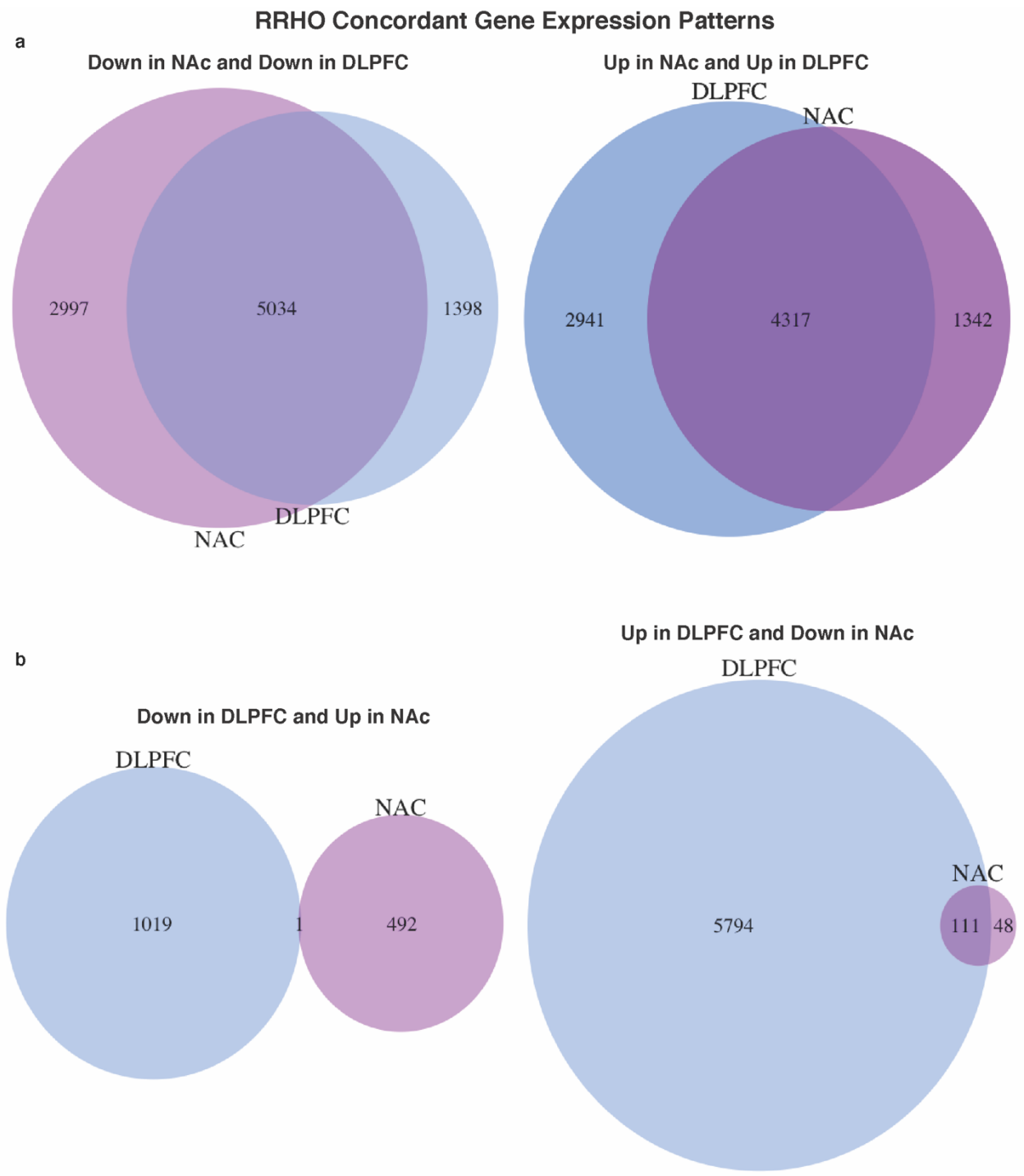

Fig. S4. Overlapping genes between DLPFC and NAc from rank-rank hypergeometic ordering analysis. (a) High overlap between DLPFC and NAc among downregulated and upregulated genes. **(b)** Low overlap between DLPFC and NAc among

genes with opposing patterns of expression (*i.e.,* downregulated in the DLPFC and upregulated in the NAc, and upregulated in the DLPFC and downregulated in the NAc).

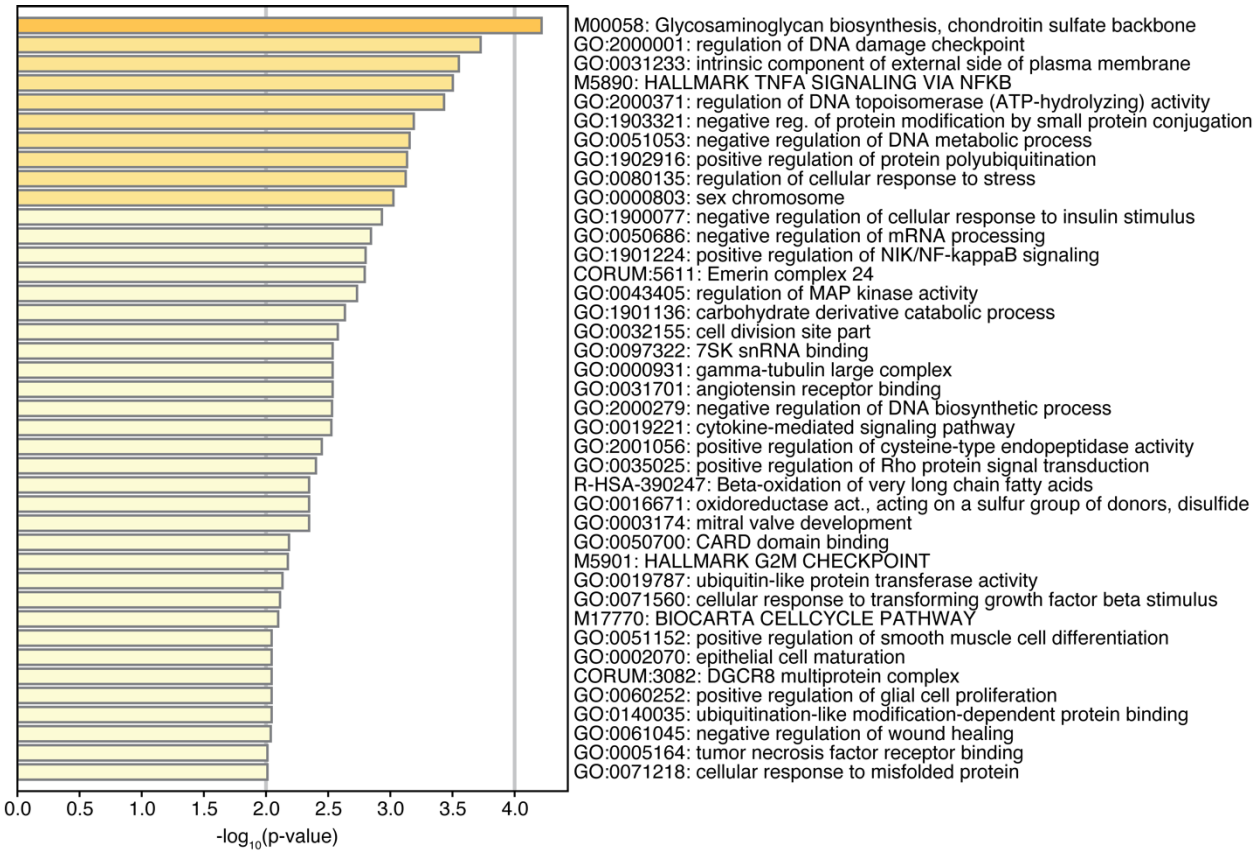

Fig. S5. Top pathways enriched from differentially expressed genes in the DLPFC and NAc of OUD subjects. All pathways significantly enriched in both the DLPFC and NAc ranked by $-\log_{10}$ p-value.

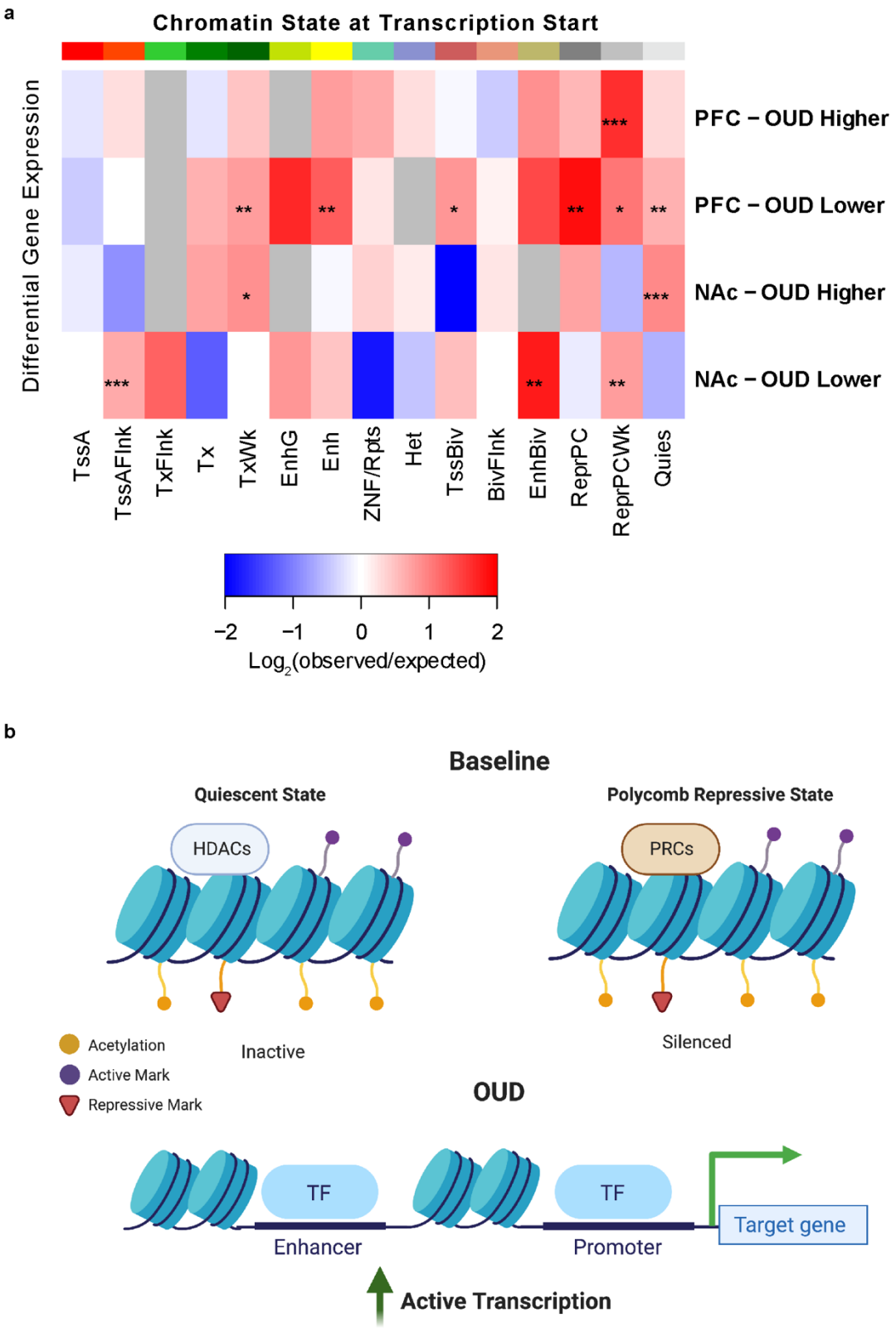
a
Chromatin State at Transcription Start
Differential Gene Expression
PFC – OUD Higher
PFC – OUD Lower
NAc – OUD Higher
NAc – OUD Lower
TssA
TssAFlnk
TxFlnk
Tx
TxWk
EnhG
Enh
ZNF/Rpts
Het
TssBiv
BivFlnk
EnhBiv
ReprPC
ReprPCWk
Quies
−2
−1
0
1
2
Log2(observed/expected)
b
Baseline
Quiescent State
Polycomb Repressive State
HDACs
PRCs
Acetylation
Active Mark
Repressive Mark
Inactive
Silenced
OUD
TF
TF
Target gene
Enhancer
Promoter
Active Transcription

811

812 **Fig. S6. Enrichment of chromatin states in differentially expressed genes in the**
813 **DLPFC and NAc of OUD subjects. (a)** Heatmap of chromatin states at transcription start
814 sites based on annotations for corresponding brain regions and enrichment of
815 upregulated and downregulated differentially expressed (DE) genes. Hypergeometric t-
816 tests were used to calculate the observed overlaps based on observed and expected
817 values. *p<0.01; **p<0.001; and ***p<0.0001. Transcription start site active (TssA);
818 Transcription start site flanking active (TssAFlnk); Transcription at gene 5' and 3' (TxFlnk);
819 Strong transcription (Tx); Weak transcription (TxWk); Genic enhancers (EnhG);
820 Enhancers (Enh); Zinc finger genes and repeats (ZNF/Rpts); Heterochromatin (Het);
821 Bivalent/poised transcription start site (TssBiv); Flanking bivalent transcription start site
822 or enhancer (EnhBiv); Repressed polycomb (ReprPC); Weak repressed polycomb
823 (ReprPCWk); Quiescent/low (Quies). **(b)** Weak polycomb repression diminishes histone
824 marks (*e.g.,* H3K27me3), which would otherwise inhibit transcription at the start site(*72*).
825 Relative to baseline, the enrichment of upregulated DE transcripts in DLPFC from OUD
826 subjects suggests that opioid induce the activation of otherwise repressed areas of the
827 genome to promote transcription. In NAc, we discovered DE transcripts were enriched for
828 genomic regions marked for a quiescent state at baseline. Quiescent states are
829 characterized by the complete absence of histone marks linked to transcriptional
830 inactivity(*72*). Similar to DLPFC, such findings suggest opioids activate otherwise inactive
831 genomic regions, resulting in transcriptional upregulation in NAc.

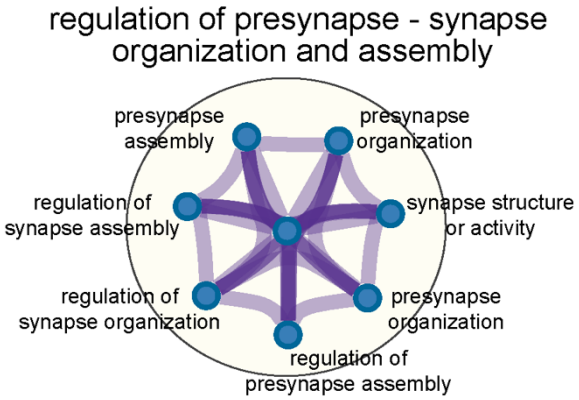

Fig S7. Enrichment of synapse-related pathways in differentially expressed transcripts significantly associated with cell-type specific markers in neurons.

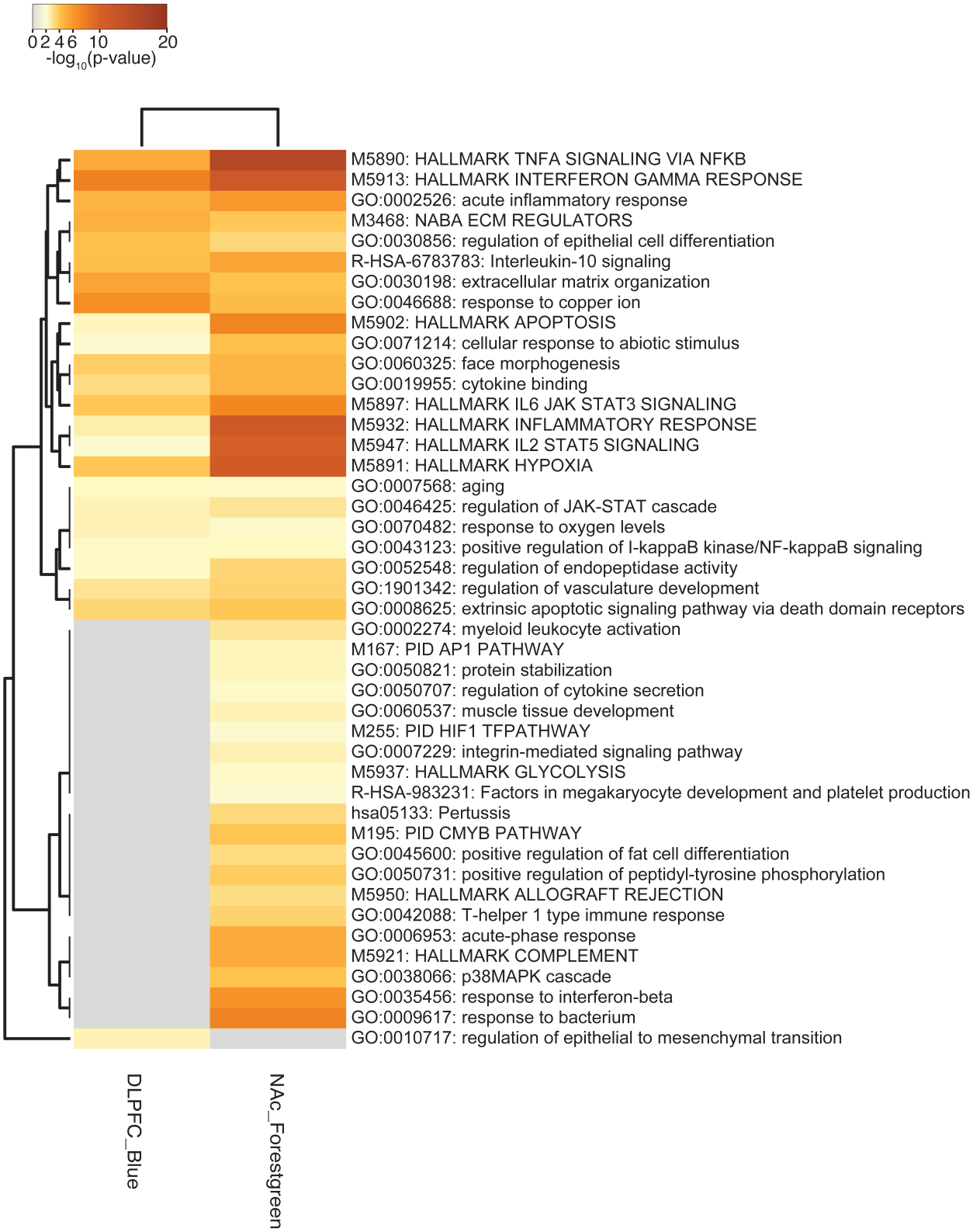
0 2 4 6 10 20
-log10(p-value)
M5890: HALLMARK TNFA SIGNALING VIA NFKB
M5913: HALLMARK INTERFERON GAMMA RESPONSE
GO:0002526: acute inflammatory response
M3468: NABA ECM REGULATORS
GO:0030856: regulation of epithelial cell differentiation
R-HSA-6783783: Interleukin-10 signaling
GO:0030198: extracellular matrix organization
GO:0046688: response to copper ion
M5902: HALLMARK APOPTOSIS
GO:0071214: cellular response to abiotic stimulus
GO:0060325: face morphogenesis
GO:0019955: cytokine binding
M5897: HALLMARK IL6 JAK STAT3 SIGNALING
M5932: HALLMARK INFLAMMATORY RESPONSE
M5947: HALLMARK IL2 STAT5 SIGNALING
M5891: HALLMARK HYPOXIA
GO:0007568: aging
GO:0046425: regulation of JAK-STAT cascade
GO:0070482: response to oxygen levels
GO:0043123: positive regulation of I-kappaB kinase/NF-kappaB signaling
GO:0052548: regulation of endopeptidase activity
GO:1901342: regulation of vasculature development
GO:0008625: extrinsic apoptotic signaling pathway via death domain receptors
GO:0002274: myeloid leukocyte activation
M167: PID AP1 PATHWAY
GO:0050821: protein stabilization
GO:0050707: regulation of cytokine secretion
GO:0060537: muscle tissue development
M255: PID HIF1 TFPATHWAY
GO:0007229: integrin-mediated signaling pathway
M5937: HALLMARK GLYCOLYSIS
R-HSA-983231: Factors in megakaryocyte development and platelet production
hsa05133: Pertussis
M195: PID CMYB PATHWAY
GO:0045600: positive regulation of fat cell differentiation
GO:0050731: positive regulation of peptidyl-tyrosine phosphorylation
M5950: HALLMARK ALLOGRAFT REJECTION
GO:0042088: T-helper 1 type immune response
GO:0006953: acute-phase response
M5921: HALLMARK COMPLEMENT
GO:0038066: p38MAPK cascade
GO:0035456: response to interferon-beta
GO:0009617: response to bacterium
GO:0010717: regulation of epithelial to mesenchymal transition
DLPFC_Blue
NAc_Forestgreen

836 **Fig. S8. Top pathways enriched from genes comprising OUD-specific blue module**
837 **in the DLPFC and forestgreen module in the NAc.** All pathways significantly enriched
838 in the NAc ranked by $-\log_{10}$ p-value. Warmer colors indicate higher enrichment. Gray
839 indicates the absence of enrichment for that particular pathway in the blue or forestgreen
840 modules.

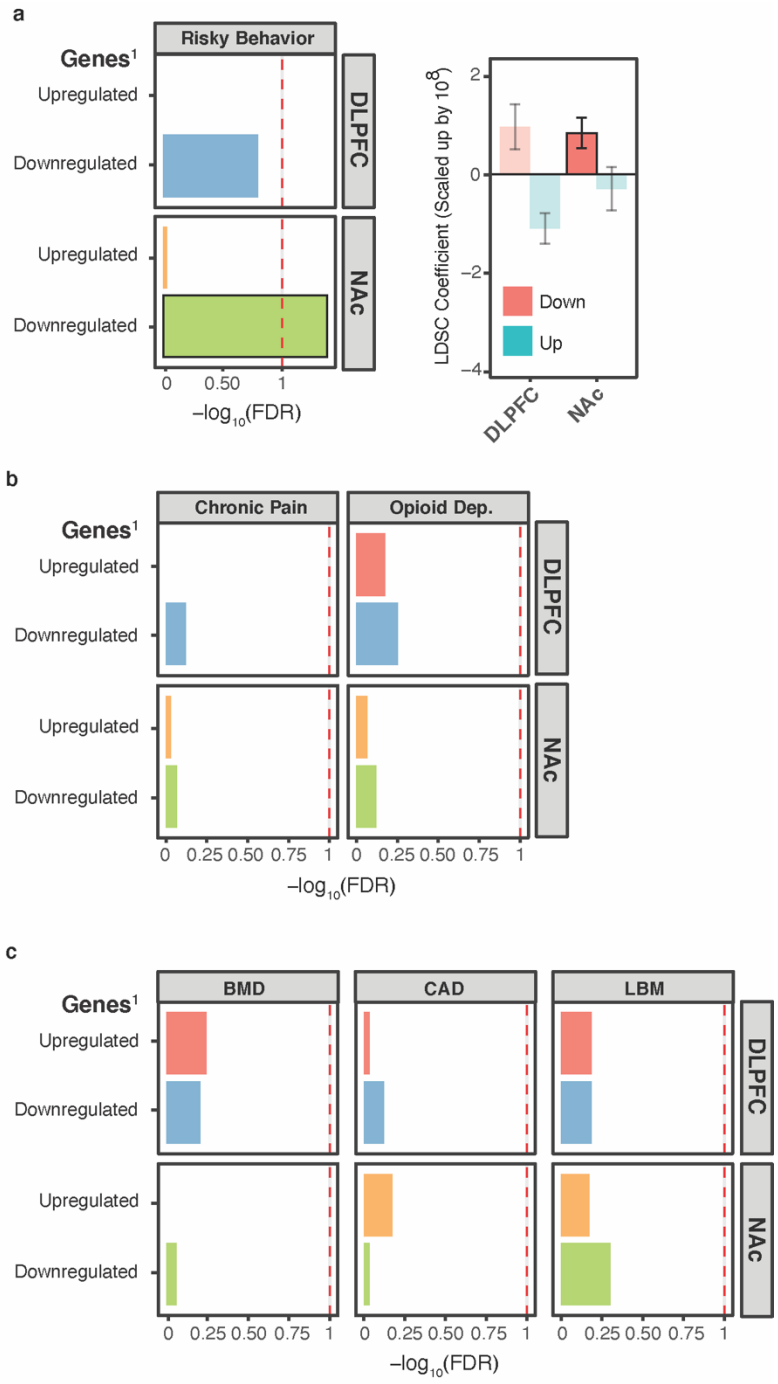

[1]Differentially expressed genes at cutoff of p<0.01 and FDR<0.1

842 **Fig. S9. Differentially expressed genes in the DLPFC and NAc enrich for genetic**
843 **liability of risky behavior.** Several well-powered genome-wide associated studies
844 (GWAS) have identified risk loci associated with substance use-related traits, including
845 smoking and risky behavior. Significant risk loci overlap with intronic and distal intergenic
846 noncoding regions, presumably within cis-acting regulatory elements of gene expression.
847 **(a)** Proximal noncoding regions of differentially expressed (DE) genes in DLPFC and NAc
848 from OUD subjects were investigated for enrichment of genetic risk variants of substance
849 use-related traits using partitioned heritability linkage-disequilibrium score regression
850 analysis. Linkage disequilibrium score correlation (LDSC) coefficients for risky behavior
851 by upregulated and downregulated DE genes within the DLPFC and NAc of OUD
852 subjects. Positive LDSC coefficients which are highlighted indicate significant enrichment
853 of downregulated DE genes in NAc. **(b)** No enrichment was found for chronic pain or
854 opioid dependence GWAS. **(c)** No enrichment was found for unrelated GWAS traits,
855 including bone mineral density (BMD), coronary artery disease (CAD), and lean body
856 mass (LBM).

857

858 **Table S1. Subject information.**

859

860 **Table S2. Differentially expressed genes by specific cell-type.** Significant
861 differentially expressed genes were only for neurons and microglia. FDR<0.05.

862

863 **Table S3. Long noncoding RNAs in DLPFC blue module and NAc forestgreen**
864 **module for control and OUD subjects.**

865

866 **Data file S1. Differentially expressed genes between DLPFC and NAc in control**
867 **subjects.**

868

869 **Data file S2. Differentially expressed genes in DLPFC.**

870

871 **Data file S3. Differentially expressed genes in NAc.**

872

873
874

875

876

877 **References:**

878

879 1. C. M. Jones, E. B. Einstein, W. M. Compton, Changes in Synthetic Opioid
880 Involvement in Drug Overdose Deaths in the United States, 2010-2016. *JAMA*
881 **319**, 1819-1821 (2018).
882 2. M. Gossop, L. Green, G. Phillips, B. Bradley, Lapse, relapse and survival among
883 opiate addicts after treatment. A prospective follow-up study. *Br J Psychiatry* **154**,
884 348-353 (1989).
885 3. G. F. Koob, Neurobiology of Opioid Addiction: Opponent Process, Hyperkatifeia,
886 and Negative Reinforcement. *Biol Psychiatry* **87**, 44-53 (2020).
887 4. B. Adinoff, L. M. Rilling, M. J. Williams, E. Schreffler, T. S. Schepis, T. Rosvall, U.
888 Rao, Impulsivity, neural deficits, and the addictions: the "oops" factor in relapse.
889 *J Addict Dis* **26 Suppl 1**, 25-39 (2007).
890 5. B. A. Baldo, Prefrontal Cortical Opioids and Dysregulated Motivation: A Network
891 Hypothesis. *Trends Neurosci* **39**, 366-377 (2016).
892 6. J. Xu, Z. Lu, M. Xu, L. Pan, Y. Deng, X. Xie, H. Liu, S. Ding, Y. L. Hurd, G. W.
893 Pasternak, R. J. Klein, L. Cartegni, W. Zhou, Y. X. Pan, A heroin addiction
894 severity-associated intronic single nucleotide polymorphism modulates
895 alternative pre-mRNA splicing of the mu opioid receptor gene OPRM1 via
896 hnRNPH interactions. *J Neurosci* **34**, 11048-11066 (2014).
897 7. T. G. Brown, J. Xu, Y. L. Hurd, Y. X. Pan, Dysregulated expression of the
898 alternatively spliced variant mRNAs of the mu opioid receptor gene, OPRM1, in
899 the medial prefrontal cortex of male human heroin abusers and heroin self-
900 administering male rats. *J Neurosci Res*, (2020).
901 8. S. E. Sillivan, J. D. Whittard, M. M. Jacobs, Y. Ren, A. R. Mazloom, F. F. Caputi,
902 M. Horvath, E. Keller, A. Ma'ayan, Y. X. Pan, L. W. Chiang, Y. L. Hurd, ELK1
903 transcription factor linked to dysregulated striatal mu opioid receptor signaling
904 network and OPRM1 polymorphism in human heroin abusers. *Biol Psychiatry* **74**,
905 511-519 (2013).
906 9. D. N. Albertson, C. J. Schmidt, G. Kapatos, M. J. Bannon, Distinctive profiles of
907 gene expression in the human nucleus accumbens associated with cocaine and
908 heroin abuse. *Neuropsychopharmacology* **31**, 2304-2312 (2006).
909 10. J. W. Koo, M. S. Mazei-Robison, Q. LaPlant, G. Egervari, K. M. Braunscheidel,
910 D. N. Adank, D. Ferguson, J. Feng, H. Sun, K. N. Scobie, D. M. Damez-Werno,
911 E. Ribeiro, C. J. Peña, D. Walker, R. C. Bagot, M. E. Cahill, S. A. R. Anderson,
912 B. Labonté, G. E. Hodes, H. Browne, B. Chadwick, A. J. Robison, V. F. Vialou, C.
913 Dias, Z. Lorsch, E. Mouzon, M. K. Lobo, D. M. Dietz, S. J. Russo, R. L. Neve, Y.
914 L. Hurd, E. J. Nestler, Epigenetic basis of opiate suppression of Bdnf gene
915 expression in the ventral tegmental area. *Nat. Neurosci.* **18**, 415-422 (2015).
916 11. C. J. Browne, A. Godino, M. Salery, E. J. Nestler, Epigenetic Mechanisms of
917 Opioid Addiction. *Biol Psychiatry* **87**, 22-33 (2020).
918 12. B. Schafer, C. Gotz, J. Dudek, A. Hessenauer, U. Matti, M. Montenarh, KIF5C: a
919 new binding partner for protein kinase CK2 with a preference for the CK2alpha'
920 subunit. *Cell Mol Life Sci* **66**, 339-349 (2009).

921 13. B. Schafer, C. Gotz, M. Montenarh, The kinesin I family member KIF5C is a
922 novel substrate for protein kinase CK2. *Biochem Biophys Res Commun* **375**,
923 179-183 (2008).
924 14. S. R. Batten, E. A. Matveeva, S. W. Whiteheart, T. C. Vanaman, G. A. Gerhardt,
925 J. T. Slevin, Linking kindling to increased glutamate release in the dentate gyrus
926 of the hippocampus through the STXBP5/tomosyn-1 gene. *Brain Behav* **7**,
927 e00795 (2017).
928 15. R. B. Cupertino, D. B. Kappel, C. E. Bandeira, J. B. Schuch, B. S. da Silva, D.
929 Muller, C. H. Bau, N. R. Mota, SNARE complex in developmental psychiatry:
930 neurotransmitter exocytosis and beyond. *J Neural Transm (Vienna)* **123**, 867-883
931 (2016).
932 16. R. N. Grishanin, J. A. Kowalchyk, V. A. Klenchin, K. Ann, C. A. Earles, E. R.
933 Chapman, R. R. Gerona, T. F. Martin, CAPS acts at a prefusion step in dense-
934 core vesicle exocytosis as a PIP2 binding protein. *Neuron* **43**, 551-562 (2004).
935 17. Y. Wang, S. Sugita, T. C. Sudhof, The RIM/NIM family of neuronal C2 domain
936 proteins. Interactions with Rab3 and a new class of Src homology 3 domain
937 proteins. *J Biol Chem* **275**, 20033-20044 (2000).
938 18. X. P. Dun, D. B. Parkinson, Classic axon guidance molecules control correct
939 nerve bridge tissue formation and precise axon regeneration. *Neural Regen Res*
940 **15**, 6-9 (2020).
941 19. M. Di Benedetto, I. Bieche, F. Deshayes, S. Vacher, S. Nouet, V. Collura, I.
942 Seitz, S. Louis, P. Pineau, D. Amsellem-Ouazana, P. O. Couraud, A. D.
943 Strosberg, D. Stoppa-Lyonnet, R. Lidereau, C. Nahmias, Structural organization
944 and expression of human MTUS1, a candidate 8p22 tumor suppressor gene
945 encoding a family of angiotensin II AT2 receptor-interacting proteins, ATIP. *Gene*
946 **380**, 127-136 (2006).
947 20. P. Sangwung, G. Zhou, L. Nayak, E. R. Chan, S. Kumar, D. W. Kang, R. Zhang,
948 X. Liao, Y. Lu, K. Sugi, H. Fujioka, H. Shi, S. D. Lapping, C. C. Ghosh, S. J.
949 Higgins, S. M. Parikh, H. Jo, M. K. Jain, KLF2 and KLF4 control endothelial
950 identity and vascular integrity. *JCI Insight* **2**, e91700 (2017).
951 21. B. Obermeier, R. Daneman, R. M. Ransohoff, Development, maintenance and
952 disruption of the blood-brain barrier. *Nat Med* **19**, 1584-1596 (2013).
953 22. K. Hamada, T. Sasaki, P. A. Koni, M. Natsui, H. Kishimoto, J. Sasaki, N. Yajima,
954 Y. Horie, G. Hasegawa, M. Naito, J. Miyazaki, T. Suda, H. Itoh, K. Nakao, T. W.
955 Mak, T. Nakano, A. Suzuki, The PTEN/PI3K pathway governs normal vascular
956 development and tumor angiogenesis. *Genes Dev* **19**, 2054-2065 (2005).
957 23. C. Chaves, F. Remiao, S. Cisternino, X. Decleves, Opioids and the Blood-Brain
958 Barrier: A Dynamic Interaction with Consequences on Drug Disposition in Brain.
959 *Curr Neuropharmacol* **15**, 1156-1173 (2017).
960 24. E. Pimentel, K. Sivalingam, M. Doke, T. Samikkannu, Effects of Drugs of Abuse
961 on the Blood-Brain Barrier: A Brief Overview. *Front Neurosci* **14**, 513 (2020).
962 25. S. Heinz, C. Benner, N. Spann, E. Bertolino, Y. C. Lin, P. Laslo, J. X. Cheng, C.
963 Murre, H. Singh, C. K. Glass, Simple combinations of lineage-determining
964 transcription factors prime cis-regulatory elements required for macrophage and
965 B cell identities. *Mol Cell* **38**, 576-589 (2010).

966 26. S. H. Chang, S. Poser, Z. Xia, A novel role for serum response factor in neuronal
967 survival. *J Neurosci* **24**, 2277-2285 (2004).
968 27. A. Assali, A. J. Harrington, C. W. Cowan, Emerging roles for MEF2 in brain
969 development and mental disorders. *Curr Opin Neurobiol* **59**, 49-58 (2019).
970 28. J. B. Dietrich, The MEF2 family and the brain: from molecules to memory. *Cell*
971 *Tissue Res* **352**, 179-190 (2013).
972 29. K. Takahashi, F. C. Liu, T. Oishi, T. Mori, N. Higo, M. Hayashi, K. Hirokawa, H.
973 Takahashi, Expression of FOXP2 in the developing monkey forebrain:
974 comparison with the expression of the genes FOXP1, PBX3, and MEIS2. *J Comp*
975 *Neurol* **509**, 180-189 (2008).
976 30. C. A. Rottkamp, K. J. Lobur, C. L. Wladyka, A. K. Lucky, S. O'Gorman, Pbx3 is
977 required for normal locomotion and dorsal horn development. *Dev Biol* **314**, 23-
978 39 (2008).
979 31. R. Batista-Brito, R. Machold, C. Klein, G. Fishell, Gene expression in cortical
980 interneuron precursors is prescient of their mature function. *Cereb Cortex* **18**,
981 2306-2317 (2008).
982 32. S. Matsuda, K. Kuwako, H. J. Okano, S. Tsutsumi, H. Aburatani, Y. Saga, Y.
983 Matsuzaki, A. Akaike, H. Sugimoto, H. Okano, Sox21 promotes hippocampal
984 adult neurogenesis via the transcriptional repression of the Hes5 gene. *J*
985 *Neurosci* **32**, 12543-12557 (2012).
986 33. N. Whittington, D. Cunningham, T. K. Le, D. De Maria, E. M. Silva, Sox21
987 regulates the progression of neuronal differentiation in a dose-dependent
988 manner. *Dev Biol* **397**, 237-247 (2015).
989 34. H. Ohba, T. Chiyoda, E. Endo, M. Yano, Y. Hayakawa, M. Sakaguchi, R. B.
990 Darnell, H. J. Okano, H. Okano, Sox21 is a repressor of neuronal differentiation
991 and is antagonized by YB-1. *Neurosci Lett* **358**, 157-160 (2004).
992 35. B. Knoll, A. Nordheim, Functional versatility of transcription factors in the nervous
993 system: the SRF paradigm. *Trends Neurosci* **32**, 432-442 (2009).
994 36. V. Vialou, J. Feng, A. J. Robison, S. M. Ku, D. Ferguson, K. N. Scobie, M. S.
995 Mazei-Robison, E. Mouzon, E. J. Nestler, Serum response factor and cAMP
996 response element binding protein are both required for cocaine induction of
997 DeltaFosB. *J Neurosci* **32**, 7577-7584 (2012).
998 37. J. M. Miano, Role of serum response factor in the pathogenesis of disease. *Lab*
999 *Invest* **90**, 1274-1284 (2010).
1000 38. A. Taylor, W. Tang, E. M. Bruscia, P. X. Zhang, A. Lin, P. Gaines, D. Wu, S.
1001 Halene, SRF is required for neutrophil migration in response to inflammation.
1002 *Blood* **123**, 3027-3036 (2014).
1003 39. G. Zhuang, C. Meng, X. Guo, P. S. Cheruku, L. Shi, H. Xu, H. Li, G. Wang, A. R.
1004 Evans, S. Safe, C. Wu, B. Zhou, A novel regulator of macrophage activation:
1005 miR-223 in obesity-associated adipose tissue inflammation. *Circulation* **125**,
1006 2892-2903 (2012).
1007 40. P. T. Nguyen, L. C. Dorman, S. Pan, I. D. Vainchtein, R. T. Han, H. Nakao-Inoue,
1008 S. E. Taloma, J. J. Barron, A. B. Molofsky, M. A. Kheirbek, A. V. Molofsky,
1009 Microglial Remodeling of the Extracellular Matrix Promotes Synapse Plasticity.
1010 *Cell*, (2020).

1011 41. R. Parakalan, B. Jiang, B. Nimmi, M. Janani, M. Jayapal, J. Lu, S. S. Tay, E. A.
1012 Ling, S. T. Dheen, Transcriptome analysis of amoeboid and ramified microglia
1013 isolated from the corpus callosum of rat brain. *BMC Neurosci* **13**, 64 (2012).
1014 42. X. Liu, N. Quan, Microglia and CNS Interleukin-1: Beyond Immunological
1015 Concepts. *Front Neurol* **9**, 8 (2018).
1016 43. Y. Xu, W. Cao, M. Zhou, C. Li, Y. Luo, H. Wang, R. Zhao, S. Jiang, J. Yang, Y.
1017 Liu, X. Wang, X. Li, W. Xiong, J. Ma, S. Peng, Z. Zeng, X. Li, M. Tan, G. Li,
1018 Inactivation of BRD7 results in impaired cognitive behavior and reduced synaptic
1019 plasticity of the medial prefrontal cortex. *Behav Brain Res* **286**, 1-10 (2015).
1020 44. S. Cohen, M. E. Greenberg, Communication between the synapse and the
1021 nucleus in neuronal development, plasticity, and disease. *Annu Rev Cell Dev Biol*
1022 **24**, 183-209 (2008).
1023 45. E. Houben, N. Hellings, B. Broux, Oncostatin M, an Underestimated Player in the
1024 Central Nervous System. *Front Immunol* **10**, 1165 (2019).
1025 46. B. Heizmann, M. Sellars, A. Macias-Garcia, S. Chan, P. Kastner, Ikaros limits
1026 follicular B cell activation by regulating B cell receptor signaling pathways.
1027 *Biochem Biophys Res Commun* **470**, 714-720 (2016).
1028 47. L. B. John, A. C. Ward, The Ikaros gene family: transcriptional regulators of
1029 hematopoiesis and immunity. *Mol Immunol* **48**, 1272-1278 (2011).
1030 48. R. M. Thomas, C. Chen, N. Chunder, L. Ma, J. Taylor, E. J. Pearce, A. D. Wells,
1031 Ikaros silences T-bet expression and interferon-gamma production during T
1032 helper 2 differentiation. *J Biol Chem* **285**, 2545-2553 (2010).
1033 49. R. Chen, Q. Zhang, X. Duan, P. York, G. D. Chen, P. Yin, H. Zhu, M. Xu, P.
1034 Chen, Q. Wu, D. Li, J. Samarut, G. Xu, P. Zhang, X. Cao, J. Li, J. Wong, The 5-
1035 Hydroxymethylcytosine (5hmC) Reader UHRF2 Is Required for Normal Levels of
1036 5hmC in Mouse Adult Brain and Spatial Learning and Memory. *J Biol Chem* **292**,
1037 4533-4543 (2017).
1038 50. M. T. Morch, S. F. Sorensen, R. Khorooshi, N. Asgari, T. Owens, Selective
1039 localization of IgG from cerebrospinal fluid to brain parenchyma. *J*
1040 *Neuroinflammation* **15**, 110 (2018).
1041 51. H. D. Jang, J. Y. Noh, J. H. Shin, J. J. Lin, S. Y. Lee, PTEN regulation by the
1042 Akt/GSK-3beta axis during RANKL signaling. *Bone* **55**, 126-131 (2013).
1043 52. L. Z. He, F. Guidez, C. Tribioli, D. Peruzzi, M. Ruthardt, A. Zelent, P. P. Pandolfi,
1044 Distinct interactions of PML-RARalpha and PLZF-RARalpha with co-repressors
1045 determine differential responses to RA in APL. *Nat Genet* **18**, 126-135 (1998).
1046 53. F. Grignani, S. De Matteis, C. Nervi, L. Tomassoni, V. Gelmetti, M. Cioce, M.
1047 Fanelli, M. Ruthardt, F. F. Ferrara, I. Zamir, C. Seiser, F. Grignani, M. A. Lazar,
1048 S. Minucci, P. G. Pelicci, Fusion proteins of the retinoic acid receptor-alpha
1049 recruit histone deacetylase in promyelocytic leukaemia. *Nature* **391**, 815-818
1050 (1998).
1051 54. J. Weng, M. N. Symons, S. M. Singh, Ethanol-responsive genes (Crtam, Zbtb16,
1052 and Mobp) located in the alcohol-QTL region of chromosome 9 are associated
1053 with alcohol preference in mice. *Alcohol Clin Exp Res* **33**, 1409-1416 (2009).
1054 55. T. Matsui, V. Nieto-Estevez, S. Kyrychenko, J. W. Schneider, J. Hsieh,
1055 Retinoblastoma protein controls growth, survival and neuronal migration in
1056 human cerebral organoids. *Development* **144**, 1025-1034 (2017).

1057 56. D. S. Latchman, POU family transcription factors in the nervous system. *J Cell*
1058 *Physiol* **179**, 126-133 (1999).
1059 57. H. H. Bendall, D. C. Scherer, C. R. Edson, D. W. Ballard, E. M. Oltz,
1060 Transcription factor NF-kappaB regulates inducible Oct-2 gene expression in
1061 precursor B lymphocytes. *J Biol Chem* **272**, 28826-28828 (1997).
1062 58. D. S. Latchman, The Oct-2 transcription factor. *Int J Biochem Cell Biol* **28**, 1081-
1063 1083 (1996).
1064 59. C. Schneider, C. E. O'Leary, R. M. Locksley, Regulation of immune responses by
1065 tuft cells. *Nat Rev Immunol* **19**, 584-593 (2019).
1066 60. I. Ahmad, D. C. Hoessli, E. Walker-Nasir, S. M. Rafik, A. R. Shakoori, D. Nasir
1067 ud, Oct-2 DNA binding transcription factor: functional consequences of
1068 phosphorylation and glycosylation. *Nucleic Acids Res* **34**, 175-184 (2006).
1069 61. C. L. Thompson, L. Ng, V. Menon, S. Martinez, C. K. Lee, K. Glattfelder, S. M.
1070 Sunkin, A. Henry, C. Lau, C. Dang, R. Garcia-Lopez, A. Martinez-Ferre, A.
1071 Pombero, J. L. R. Rubenstein, W. B. Wakeman, J. Hohmann, N. Dee, A. J. Sodt,
1072 R. Young, K. Smith, T. N. Nguyen, J. Kidney, L. Kuan, A. Jeromin, A. Kaykas, J.
1073 Miller, D. Page, G. Orta, A. Bernard, Z. Riley, S. Smith, P. Wohnoutka, M. J.
1074 Hawrylycz, L. Puelles, A. R. Jones, A high-resolution spatiotemporal atlas of
1075 gene expression of the developing mouse brain. *Neuron* **83**, 309-323 (2014).
1076 62. K. Oishi, M. Aramaki, K. Nakajima, Mutually repressive interaction between
1077 Brn1/2 and Rorb contributes to the establishment of neocortical layer 2/3 and
1078 layer 4. *Proc Natl Acad Sci U S A* **113**, 3371-3376 (2016).
1079 63. D. Yue, J. Zhao, H. Chen, M. Guo, C. Chen, Y. Zhou, L. Xu, MicroRNA-7,
1080 synergizes with RORalpha, negatively controls the pathology of brain tissue
1081 inflammation. *J Neuroinflammation* **17**, 28 (2020).
1082 64. N. Journiac, S. Jolly, C. Jarvis, V. Gautheron, M. Rogard, A. Trembleau, J. P.
1083 Blondeau, J. Mariani, B. Vernet-der Garabedian, The nuclear receptor
1084 ROR(alpha) exerts a bi-directional regulation of IL-6 in resting and reactive
1085 astrocytes. *Proc Natl Acad Sci U S A* **106**, 21365-21370 (2009).
1086 65. P. Delerive, D. Monte, G. Dubois, F. Trottein, J. Fruchart-Najib, J. Mariani, J. C.
1087 Fruchart, B. Staels, The orphan nuclear receptor ROR alpha is a negative
1088 regulator of the inflammatory response. *EMBO Rep* **2**, 42-48 (2001).
1089 66. C. J. Evans, C. M. Cahill, Neurobiology of opioid dependence in creating
1090 addiction vulnerability. *F1000Res* **5**, (2016).
1091 67. J. Le Merrer, J. A. Becker, K. Befort, B. L. Kieffer, Reward processing by the
1092 opioid system in the brain. *Physiol Rev* **89**, 1379-1412 (2009).
1093 68. E. J. Nestler, Molecular mechanisms of opiate and cocaine addiction. *Curr Opin*
1094 *Neurobiol* **7**, 713-719 (1997).
1095 69. E. J. Nestler, Historical review: Molecular and cellular mechanisms of opiate and
1096 cocaine addiction. *Trends Pharmacol Sci* **25**, 210-218 (2004).
1097 70. S. B. Plaisier, R. Taschereau, J. A. Wong, T. G. Graeber, Rank-rank
1098 hypergeometric overlap: identification of statistically significant overlap between
1099 gene-expression signatures. *Nucleic Acids Res* **38**, e169 (2010).
1100 71. K. M. Cahill, Z. Huo, G. C. Tseng, R. W. Logan, M. L. Seney, Improved
1101 identification of concordant and discordant gene expression signatures using an
1102 updated rank-rank hypergeometric overlap approach. *Sci Rep* **8**, 9588 (2018).

1103 72. C. Roadmap Epigenomics, A. Kundaje, W. Meuleman, J. Ernst, M. Bilenky, A.
1104 Yen, A. Heravi-Moussavi, P. Kheradpour, Z. Zhang, J. Wang, M. J. Ziller, V.
1105 Amin, J. W. Whitaker, M. D. Schultz, L. D. Ward, A. Sarkar, G. Quon, R. S.
1106 Sandstrom, M. L. Eaton, Y. C. Wu, A. R. Pfenning, X. Wang, M. Claussnitzer, Y.
1107 Liu, C. Coarfa, R. A. Harris, N. Shoresh, C. B. Epstein, E. Gjoneska, D. Leung,
1108 W. Xie, R. D. Hawkins, R. Lister, C. Hong, P. Gascard, A. J. Mungall, R. Moore,
1109 E. Chuah, A. Tam, T. K. Canfield, R. S. Hansen, R. Kaul, P. J. Sabo, M. S.
1110 Bansal, A. Carles, J. R. Dixon, K. H. Farh, S. Feizi, R. Karlic, A. R. Kim, A.
1111 Kulkarni, D. Li, R. Lowdon, G. Elliott, T. R. Mercer, S. J. Neph, V. Onuchic, P.
1112 Polak, N. Rajagopal, P. Ray, R. C. Sallari, K. T. Siebenthall, N. A. Sinnott-
1113 Armstrong, M. Stevens, R. E. Thurman, J. Wu, B. Zhang, X. Zhou, A. E.
1114 Beaudet, L. A. Boyer, P. L. De Jager, P. J. Farnham, S. J. Fisher, D. Haussler, S.
1115 J. Jones, W. Li, M. A. Marra, M. T. McManus, S. Sunyaev, J. A. Thomson, T. D.
1116 Tlsty, L. H. Tsai, W. Wang, R. A. Waterland, M. Q. Zhang, L. H. Chadwick, B. E.
1117 Bernstein, J. F. Costello, J. R. Ecker, M. Hirst, A. Meissner, A. Milosavljevic, B.
1118 Ren, J. A. Stamatoyannopoulos, T. Wang, M. Kellis, Integrative analysis of 111
1119 reference human epigenomes. *Nature* **518**, 317-330 (2015).
1120 73. S. C. Zheng, C. E. Breeze, S. Beck, A. E. Teschendorff, Identification of
1121 differentially methylated cell types in epigenome-wide association studies. *Nat*
1122 *Methods* **15**, 1059-1066 (2018).
1123 74. K. Saijo, J. G. Collier, A. C. Li, J. A. Katzenellenbogen, C. K. Glass, An ADIOL-
1124 ERbeta-CtBP transrepression pathway negatively regulates microglia-mediated
1125 inflammation. *Cell* **145**, 584-595 (2011).
1126 75. A. Spooren, K. Kolmus, G. Laureys, R. Clinckers, J. De Keyser, G. Haegeman,
1127 S. Gerlo, Interleukin-6, a mental cytokine. *Brain Res Rev* **67**, 157-183 (2011).
1128 76. J. T. Zelikoff, N. L. Parmalee, K. Corbett, T. Gordon, C. B. Klein, M. Aschner,
1129 Microglia Activation and Gene Expression Alteration of Neurotrophins in the
1130 Hippocampus Following Early-Life Exposure to E-Cigarette Aerosols in a Murine
1131 Model. *Toxicol Sci* **162**, 276-286 (2018).
1132 77. M. Tufano, G. Pinna, Is There a Future for PPARs in the Treatment of
1133 Neuropsychiatric Disorders? *Molecules* **25**, (2020).
1134 78. R. H. Shih, C. Y. Wang, C. M. Yang, NF-kappaB Signaling Pathways in
1135 Neurological Inflammation: A Mini Review. *Front Mol Neurosci* **8**, 77 (2015).
1136 79. E. Butturini, D. Boriero, A. Carcereri de Prati, S. Mariotto, STAT1 drives M1
1137 microglia activation and neuroinflammation under hypoxia. *Arch Biochem*
1138 *Biophys* **669**, 22-30 (2019).
1139 80. X. R. Mao, A. M. Moerman-Herzog, Y. Chen, S. W. Barger, Unique aspects of
1140 transcriptional regulation in neurons--nuances in NFkappaB and Sp1-related
1141 factors. *J Neuroinflammation* **6**, 16 (2009).
1142 81. H. Wang, J. Brown, S. Gao, S. Liang, R. Jotwani, H. Zhou, J. Suttles, D. A. Scott,
1143 R. J. Lamont, The role of JAK-3 in regulating TLR-mediated inflammatory
1144 cytokine production in innate immune cells. *J Immunol* **191**, 1164-1174 (2013).
1145 82. Y. J. Choi, S. Kim, Y. Choi, T. B. Nielsen, J. Yan, A. Lu, J. Ruan, H. R. Lee, H.
1146 Wu, B. Spellberg, J. U. Jung, SERPINB1-mediated checkpoint of inflammatory
1147 caspase activation. *Nat Immunol* **20**, 276-287 (2019).

1148 83. H. S. Huang, X. Y. Huang, H. Z. Yu, Y. Xue, P. L. Zhu, Circular RNA circ-RELL1
1149 regulates inflammatory response by miR-6873-3p/MyD88/NF-kappaB axis in
1150 endothelial cells. *Biochem Biophys Res Commun* **525**, 512-519 (2020).
1151 84. A. Luz, N. Fainstein, O. Einstein, T. Ben-Hur, The role of CNS TLR2 activation in
1152 mediating innate versus adaptive neuroinflammation. *Exp Neurol* **273**, 234-242
1153 (2015).
1154 85. H. Zelova, J. Hosek, TNF-alpha signalling and inflammation: interactions
1155 between old acquaintances. *Inflamm Res* **62**, 641-651 (2013).
1156 86. H. S. Kim, H. Sohn, S. W. Jang, G. R. Lee, The transcription factor NFIL3
1157 controls regulatory T-cell function and stability. *Exp Mol Med* **51**, 80 (2019).
1158 87. D. B. Rosen, W. Cao, D. T. Avery, S. G. Tangye, Y. J. Liu, J. P. Houchins, L. L.
1159 Lanier, Functional consequences of interactions between human NKR-P1A and
1160 its ligand LLT1 expressed on activated dendritic cells and B cells. *J Immunol* **180**,
1161 6508-6517 (2008).
1162 88. C. Germain, A. Meier, T. Jensen, P. Knapnougel, G. Poupon, A. Lazzari, A.
1163 Neisig, K. Hakansson, T. Dong, N. Wagtmann, E. D. Galsgaard, P. Spee, V. M.
1164 Braud, Induction of lectin-like transcript 1 (LLT1) protein cell surface expression
1165 by pathogens and interferon-gamma contributes to modulate immune responses.
1166 *J Biol Chem* **286**, 37964-37975 (2011).
1167 89. M. S. Moodbidri, N. V. Shirsat, Induction of BAALC and down regulation of
1168 RAMP3 in astrocytes treated with differentiation inducers. *Cell Biol Int* **30**, 210-
1169 213 (2006).
1170 90. A. Cooke, T. Schwarzl, I. Huppertz, G. Kramer, P. Mantas, A. M. Alleaume, W.
1171 Huber, J. Krijgsveld, M. W. Hentze, The RNA-Binding Protein YBX3 Controls
1172 Amino Acid Levels by Regulating SLC mRNA Abundance. *Cell Rep* **27**, 3097-
1173 3106 e3095 (2019).
1174 91. N. Singh, G. F. Ecker, Insights into the Structure, Function, and Ligand Discovery
1175 of the Large Neutral Amino Acid Transporter 1, LAT1. *Int J Mol Sci* **19**, (2018).
1176 92. M. H. Saad, M. Rumschlag, M. H. Guerra, C. L. Savonen, A. M. Jaster, P. D.
1177 Olson, A. Alazizi, F. Luca, R. Pique-Regi, C. J. Schmidt, M. J. Bannon,
1178 Differentially expressed gene networks, biomarkers, long noncoding RNAs, and
1179 shared responses with cocaine identified in the midbrains of human opioid
1180 abusers. *Sci Rep* **9**, 1534 (2019).
1181 93. R. Karlsson Linner, P. Biroli, E. Kong, S. F. W. Meddens, R. Wedow, M. A.
1182 Fontana, M. Lebreton, S. P. Tino, A. Abdellaoui, A. R. Hammerschlag, M. G.
1183 Nivard, A. Okbay, C. A. Rietveld, P. N. Timshel, M. Trzaskowski, R. Vlaming, C.
1184 L. Zund, Y. Bao, L. Buzdugan, A. H. Caplin, C. Y. Chen, P. Eibich, P. Fontanillas,
1185 J. R. Gonzalez, P. K. Joshi, V. Karhunen, A. Kleinman, R. Z. Levin, C. M. Lill, G.
1186 A. Meddens, G. Muntane, S. Sanchez-Roige, F. J. V. Rooij, E. Taskesen, Y. Wu,
1187 F. Zhang, T. and Me Research, Q. C. e, C. International Cannabis, C. Social
1188 Science Genetic Association, A. Auton, J. D. Boardman, D. W. Clark, A. Conlin,
1189 C. C. Dolan, U. Fischbacher, P. J. F. Groenen, K. M. Harris, G. Hasler, A.
1190 Hofman, M. A. Ikram, S. Jain, R. Karlsson, R. C. Kessler, M. Kooyman, J.
1191 MacKillop, M. Mannikko, C. Morcillo-Suarez, M. B. McQueen, K. M. Schmidt, M.
1192 C. Smart, M. Sutter, A. R. Thurik, A. G. Uitterlinden, J. White, H. Wit, J. Yang, L.
1193 Bertram, D. I. Boomsma, T. Esko, E. Fehr, D. A. Hinds, M. Johannesson, M.

Kumari, D. Laibson, P. K. E. Magnusson, M. N. Meyer, A. Navarro, A. A. Palmer, T. H. Pers, D. Posthuma, D. Schunk, M. B. Stein, R. Svento, H. Tiemeier, P. Timmers, P. Turley, R. J. Ursano, G. G. Wagner, J. F. Wilson, J. Gratten, J. J. Lee, D. Cesarini, D. J. Benjamin, P. D. Koellinger, J. P. Beauchamp, Genome-wide association analyses of risk tolerance and risky behaviors in over 1 million individuals identify hundreds of loci and shared genetic influences. *Nat Genet* **51**, 245-257 (2019).

94. M. Liu, Y. Jiang, R. Wedow, Y. Li, D. M. Brazel, F. Chen, G. Datta, J. Davila-Velderrain, D. McGuire, C. Tian, X. Zhan, T. andMe Research, H. A.-I. Psychiatry, H. Choquet, A. R. Docherty, J. D. Faul, J. R. Foerster, L. G. Fritsche, M. E. Gabrielsen, S. D. Gordon, J. Haessler, J. J. Hottenga, H. Huang, S. K. Jang, P. R. Jansen, Y. Ling, R. Magi, N. Matoba, G. McMahon, A. Mulas, V. Orru, T. Palviainen, A. Pandit, G. W. Reginsson, A. H. Skogholt, J. A. Smith, A. E. Taylor, C. Turman, G. Willemsen, H. Young, K. A. Young, G. J. M. Zajac, W. Zhao, W. Zhou, G. Bjornsdottir, J. D. Boardman, M. Boehnke, D. I. Boomsma, C. Chen, F. Cucca, G. E. Davies, C. B. Eaton, M. A. Ehringer, T. Esko, E. Fiorillo, N. A. Gillespie, D. F. Gudbjartsson, T. Haller, K. M. Harris, A. C. Heath, J. K. Hewitt, I. B. Hickie, J. E. Hokanson, C. J. Hopfer, D. J. Hunter, W. G. Iacono, E. O. Johnson, Y. Kamatani, S. L. R. Kardia, M. C. Keller, M. Kellis, C. Kooperberg, P. Kraft, K. S. Krauter, M. Laakso, P. A. Lind, A. Loukola, S. M. Lutz, P. A. F. Madden, N. G. Martin, M. McGue, M. B. McQueen, S. E. Medland, A. Metspalu, K. L. Mohlke, J. B. Nielsen, Y. Okada, U. Peters, T. J. C. Polderman, D. Posthuma, A. P. Reiner, J. P. Rice, E. Rimm, R. J. Rose, V. Runarsdottir, M. C. Stallings, A. Stancakova, H. Stefansson, K. K. Thai, H. A. Tindle, T. Tyrfingsson, T. L. Wall, D. R. Weir, C. Weisner, J. B. Whitfield, B. S. Winsvold, J. Yin, L. Zuccolo, L. J. Bierut, K. Hveem, J. J. Lee, M. R. Munafo, N. L. Saccone, C. J. Willer, M. C. Cornelis, S. P. David, D. A. Hinds, E. Jorgenson, J. Kaprio, J. A. Stitzel, K. Stefansson, T. E. Thorgeirsson, G. Abecasis, D. J. Liu, S. Vrieze, Association studies of up to 1.2 million individuals yield new insights into the genetic etiology of tobacco and alcohol use. *Nat Genet* **51**, 237-244 (2019).

95. J. A. Pasman, K. J. H. Verweij, Z. Gerring, S. Stringer, S. Sanchez-Roige, J. L. Treur, A. Abdellaoui, M. G. Nivard, B. M. L. Baselmans, J. S. Ong, H. F. Ip, M. D. van der Zee, M. Bartels, F. R. Day, P. Fontanillas, S. L. Elson, T. andMe Research, H. de Wit, L. K. Davis, J. MacKillop, C. Substance Use Disorders Working Group of the Psychiatric Genomics, C. International Cannabis, J. L. Derringer, S. J. T. Branje, C. A. Hartman, A. C. Heath, P. A. C. van Lier, P. A. F. Madden, R. Magi, W. Meeus, G. W. Montgomery, A. J. Oldehinkel, Z. Pausova, J. A. Ramos-Quiroga, T. Paus, M. Ribases, J. Kaprio, M. P. M. Boks, J. T. Bell, T. D. Spector, J. Gelernter, D. I. Boomsma, N. G. Martin, S. MacGregor, J. R. B. Perry, A. A. Palmer, D. Posthuma, M. R. Munafo, N. A. Gillespie, E. M. Derks, J. M. Vink, Author Correction: GWAS of lifetime cannabis use reveals new risk loci, genetic overlap with psychiatric traits, and a causal effect of schizophrenia liability. *Nat Neurosci* **22**, 1196 (2019).

96. R. S. Hofford, S. J. Russo, D. D. Kiraly, Neuroimmune mechanisms of psychostimulant and opioid use disorders. *Eur J Neurosci* **50**, 2562-2573 (2019).

1239 97. A. Suzumura, A. Ito, M. Yoshikawa, M. Sawada, Ibudilast suppresses TNFalpha
1240 production by glial cells functioning mainly as type III phosphodiesterase inhibitor
1241 in the CNS. *Brain Res* **837**, 203-212 (1999).
1242 98. Z. D. Cooper, K. W. Johnson, M. Pavlicova, A. Glass, S. K. Vosburg, M. A.
1243 Sullivan, J. M. Manubay, D. M. Martinez, J. D. Jones, P. A. Saccone, S. D.
1244 Comer, The effects of ibudilast, a glial activation inhibitor, on opioid withdrawal
1245 symptoms in opioid-dependent volunteers. *Addict Biol* **21**, 895-903 (2016).
1246 99. V. E. Metz, J. D. Jones, J. Manubay, M. A. Sullivan, S. Mogali, A. Segoshi, G.
1247 Madera, K. W. Johnson, S. D. Comer, Effects of Ibudilast on the Subjective,
1248 Reinforcing, and Analgesic Effects of Oxycodone in Recently Detoxified Adults
1249 with Opioid Dependence. *Neuropsychopharmacology* **42**, 1825-1832 (2017).
1250 100. S. T. Bland, M. R. Hutchinson, S. F. Maier, L. R. Watkins, K. W. Johnson, The
1251 glial activation inhibitor AV411 reduces morphine-induced nucleus accumbens
1252 dopamine release. *Brain Behav Immun* **23**, 492-497 (2009).
1253 101. M. R. Hutchinson, A. L. Northcutt, L. W. Chao, J. J. Kearney, Y. Zhang, D. L.
1254 Berkelhammer, L. C. Loram, R. R. Rozeske, S. T. Bland, S. F. Maier, T. T.
1255 Gleeson, L. R. Watkins, Minocycline suppresses morphine-induced respiratory
1256 depression, suppresses morphine-induced reward, and enhances systemic
1257 morphine-induced analgesia. *Brain Behav Immun* **22**, 1248-1256 (2008).
1258 102. G. de Guglielmo, M. Melis, M. A. De Luca, M. Kallupi, H. W. Li, K. Niswender, A.
1259 Giordano, M. Senzacqua, L. Somaini, A. Cippitelli, G. Gaitanaris, G. Demopulos,
1260 R. Damadzic, J. Tapocik, M. Heilig, R. Ciccocioppo, PPARgamma activation
1261 attenuates opioid consumption and modulates mesolimbic dopamine
1262 transmission. *Neuropsychopharmacology* **40**, 927-937 (2015).
1263 103. F. R. Theberge, X. Li, S. Kambhampati, C. L. Pickens, R. St Laurent, J. M.
1264 Bossert, M. H. Baumann, M. R. Hutchinson, K. C. Rice, L. R. Watkins, Y.
1265 Shaham, Effect of chronic delivery of the Toll-like receptor 4 antagonist (+)-
1266 naltrexone on incubation of heroin craving. *Biol Psychiatry* **73**, 729-737 (2013).
1267 104. R. K. Bachtell, J. D. Jones, K. G. Heinzerling, P. M. Beardsley, S. D. Comer, Glial
1268 and neuroinflammatory targets for treating substance use disorders. *Drug*
1269 *Alcohol Depend* **180**, 156-170 (2017).
1270 105. L. N. Eidson, K. Inoue, L. J. Young, M. G. Tansey, A. Z. Murphy, Toll-like
1271 Receptor 4 Mediates Morphine-Induced Neuroinflammation and Tolerance via
1272 Soluble Tumor Necrosis Factor Signaling. *Neuropsychopharmacology* **42**, 661-
1273 670 (2017).
1274 106. E. M. Lefevre, M. T. Pisansky, C. Toddes, F. Baruffaldi, M. Pravetoni, L. Tian, T.
1275 J. Y. Kono, P. E. Rothwell, Interruption of continuous opioid exposure
1276 exacerbates drug-evoked adaptations in the mesolimbic dopamine system.
1277 *Neuropsychopharmacology*, (2020).
1278 107. M. Corkrum, P. E. Rothwell, M. J. Thomas, P. Kofuji, A. Araque, Opioid-Mediated
1279 Astrocyte-Neuron Signaling in the Nucleus Accumbens. *Cells* **8**, (2019).
1280 108. A. Oeckinghaus, S. Ghosh, The NF-kappaB family of transcription factors and its
1281 regulation. *Cold Spring Harb Perspect Biol* **1**, a000034 (2009).
1282 109. S. Ghosh, M. J. May, E. B. Kopp, NF-kappa B and Rel proteins: evolutionarily
1283 conserved mediators of immune responses. *Annu Rev Immunol* **16**, 225-260
1284 (1998).

1285 110. K. Lieb, B. L. Fiebich, M. Berger, J. Bauer, K. Schulze-Osthoff, The neuropeptide
1286 substance P activates transcription factor NF-kappa B and kappa B-dependent
1287 gene expression in human astrocytoma cells. *J Immunol* **159**, 4952-4958 (1997).
1288 111. X. Wang, S. D. Douglas, K. G. Commons, D. E. Pleasure, J. Lai, C. Ho, P.
1289 Bannerman, M. Williams, W. Ho, A non-peptide substance P antagonist (CP-
1290 96,345) inhibits morphine-induced NF-kappa B promoter activation in human
1291 NT2-N neurons. *J Neurosci Res* **75**, 544-553 (2004).
1292 112. J. Sun, R. D. Ramnath, L. Zhi, R. Tamizhselvi, M. Bhatia, Substance P enhances
1293 NF-kappaB transactivation and chemokine response in murine macrophages via
1294 ERK1/2 and p38 MAPK signaling pathways. *Am J Physiol Cell Physiol* **294**,
1295 C1586-1596 (2008).
1296 113. B. E. Sawaya, S. L. Deshmane, R. Mukerjee, S. Fan, K. Khalili, TNF alpha
1297 production in morphine-treated human neural cells is NF-kappaB-dependent. *J*
1298 *Neuroimmune Pharmacol* **4**, 140-149 (2009).
1299 114. Y. N. Hou, M. Vlaskovska, G. Cebers, L. Kasakov, S. Liljequist, L. Terenius, A
1300 mu-receptor opioid agonist induces AP-1 and NF-kappa B transcription factor
1301 activity in primary cultures of rat cortical neurons. *Neurosci Lett* **212**, 159-162
1302 (1996).
1303 115. A. K. Rehni, P. Bhateja, T. G. Singh, N. Singh, Nuclear factor-kappa-B inhibitor
1304 modulates the development of opioid dependence in a mouse model of
1305 naloxone-induced opioid withdrawal syndrome. *Behav Pharmacol* **19**, 265-269
1306 (2008).
1307 116. J. Kraus, C. Borner, E. Giannini, V. Hollt, The role of nuclear factor kappaB in
1308 tumor necrosis factor-regulated transcription of the human mu-opioid receptor
1309 gene. *Mol Pharmacol* **64**, 876-884 (2003).
1310 117. K. P. Karalis, M. Venihaki, J. Zhao, L. E. van Vlerken, C. Chandras, NF-kappaB
1311 participates in the corticotropin-releasing, hormone-induced regulation of the
1312 pituitary proopiomelanocortin gene. *J Biol Chem* **279**, 10837-10840 (2004).
1313 118. Y. L. Chen, P. Y. Law, H. H. Loh, Action of NF-kappaB on the delta opioid
1314 receptor gene promoter. *Biochem Biophys Res Commun* **352**, 818-822 (2007).
1315 119. A. Rattner, M. Korner, H. Rosen, P. A. Baeuerle, Y. Citri, Nuclear factor kappa B
1316 activates proenkephalin transcription in T lymphocytes. *Mol Cell Biol* **11**, 1017-
1317 1022 (1991).
1318 120. S. Simeonidis, I. Castagliuolo, A. Pan, J. Liu, C. C. Wang, A. Mykoniatis, A.
1319 Pasha, L. Valenick, S. Sougioultzis, D. Zhao, C. Pothoulakis, Regulation of the
1320 NK-1 receptor gene expression in human macrophage cells via an NF-kappa B
1321 site on its promoter. *Proc Natl Acad Sci U S A* **100**, 2957-2962 (2003).
1322 121. X. Zhang, Y. Cui, J. Jing, Y. Cui, W. Xin, X. Liu, Involvement of p38/NF-kappaB
1323 signaling pathway in the nucleus accumbens in the rewarding effects of morphine
1324 in rats. *Behav Brain Res* **218**, 184-189 (2011).
1325 122. Y. L. Chen, P. Y. Law, H. H. Loh, Nuclear factor kappaB signaling in opioid
1326 functions and receptor gene expression. *J Neuroimmune Pharmacol* **1**, 270-279
1327 (2006).
1328 123. D. M. Mosser, J. P. Edwards, Exploring the full spectrum of macrophage
1329 activation. *Nat Rev Immunol* **8**, 958-969 (2008).

124. A. C. Murphy, S. J. Lalor, M. A. Lynch, K. H. Mills, Infiltration of Th1 and Th17 cells and activation of microglia in the CNS during the course of experimental autoimmune encephalomyelitis. *Brain Behav Immun* **24**, 641-651 (2010).
125. T. T. Ta, H. O. Dikmen, S. Schilling, B. Chausse, A. Lewen, J. O. Hollnagel, O. Kann, Priming of microglia with IFN-gamma slows neuronal gamma oscillations in situ. *Proc Natl Acad Sci U S A* **116**, 4637-4642 (2019).
126. C. Dejean, T. Boraud, C. Le Moine, Opiate dependence induces network state shifts in the limbic system. *Neurobiol Dis* **59**, 220-229 (2013).
127. T. K. Eisenstein, The Role of Opioid Receptors in Immune System Function. *Front Immunol* **10**, 2904 (2019).
128. K. Valentinova, A. Tchenio, M. Trusel, J. A. Clerke, A. L. Lalive, S. Tzanoulinou, A. Matera, I. Moutkine, L. Maroteaux, R. C. Paolicelli, A. Volterra, C. Bellone, M. Mameli, Morphine withdrawal recruits lateral habenula cytokine signaling to reduce synaptic excitation and sociability. *Nat Neurosci* **22**, 1053-1056 (2019).
129. K. Kangwantas, E. Pinteaux, J. Penny, The extracellular matrix protein laminin-10 promotes blood-brain barrier repair after hypoxia and inflammation in vitro. *J Neuroinflammation* **13**, 25 (2016).
130. A. Faissner, J. Reinhard, The extracellular matrix compartment of neural stem and glial progenitor cells. *Glia* **63**, 1330-1349 (2015).
131. A. Dityatev, M. Schachner, P. Sonderegger, The dual role of the extracellular matrix in synaptic plasticity and homeostasis. *Nat Rev Neurosci* **11**, 735-746 (2010).
132. S. Franitza, R. Hershkoviz, N. Kam, N. Lichtenstein, G. G. Vaday, R. Alon, O. Lider, TNF-alpha associated with extracellular matrix fibronectin provides a stop signal for chemotactically migrating T cells. *J Immunol* **165**, 2738-2747 (2000).
133. E. H. Camejo, B. Rosengren, G. Camejo, P. Sartipy, G. Fager, G. Bondjers, Interferon gamma binds to extracellular matrix chondroitin-sulfate proteoglycans, thus enhancing its cellular response. *Arterioscler Thromb Vasc Biol* **15**, 1456-1465 (1995).
134. H. P. Li, Y. Komuta, J. Kimura-Kuroda, T. H. van Kuppevelt, H. Kawano, Roles of chondroitin sulfate and dermatan sulfate in the formation of a lesion scar and axonal regeneration after traumatic injury of the mouse brain. *J Neurotrauma* **30**, 413-425 (2013).
135. A. Kruyer, V. C. Chioma, P. W. Kalivas, The Opioid-Addicted Tetrapartite Synapse. *Biol Psychiatry* **87**, 34-43 (2020).
136. P. D. Smith, V. J. Coulson-Thomas, S. Foscarin, J. C. Kwok, J. W. Fawcett, "GAG-ing with the neuron": The role of glycosaminoglycan patterning in the central nervous system. *Exp Neurol* **274**, 100-114 (2015).
137. D. E. Harlow, W. B. Macklin, Inhibitors of myelination: ECM changes, CSPGs and PTPs. *Exp Neurol* **251**, 39-46 (2014).
138. J. C. Pendleton, M. J. Shamblott, D. S. Gary, V. Belegu, A. Hurtado, M. L. Malone, J. W. McDonald, Chondroitin sulfate proteoglycans inhibit oligodendrocyte myelination through PTPsigma. *Exp Neurol* **247**, 113-121 (2013).

139. E. Bora, M. Yucel, A. Fornito, C. Pantelis, B. J. Harrison, L. Cocchi, G. Pell, D. I. Lubman, White matter microstructure in opiate addiction. *Addict Biol* **17**, 141-148 (2012).
140. W. Li, J. Zhu, Q. Li, J. Ye, J. Chen, J. Liu, Z. Li, Y. Li, X. Yan, Y. Wang, W. Wang, Brain white matter integrity in heroin addicts during methadone maintenance treatment is related to relapse propensity. *Brain Behav* **6**, e00436 (2016).
141. H. Liu, L. Li, Y. Hao, D. Cao, L. Xu, R. Rohrbaugh, Z. Xue, W. Hao, B. Shan, Z. Liu, Disrupted white matter integrity in heroin dependence: a controlled study utilizing diffusion tensor imaging. *Am J Drug Alcohol Abuse* **34**, 562-575 (2008).
142. J. Upadhyay, N. Maleki, J. Potter, I. Elman, D. Rudrauf, J. Knudsen, D. Wallin, G. Pendse, L. McDonald, M. Griffin, J. Anderson, L. Nutile, P. Renshaw, R. Weiss, L. Becerra, D. Borsook, Alterations in brain structure and functional connectivity in prescription opioid-dependent patients. *Brain* **133**, 2098-2114 (2010).
143. Y. Wang, W. Li, Q. Li, W. Yang, J. Zhu, W. Wang, White matter impairment in heroin addicts undergoing methadone maintenance treatment and prolonged abstinence: a preliminary DTI study. *Neurosci Lett* **494**, 49-53 (2011).
144. D. Avey, S. Sankararaman, A. K. Y. Yim, R. Barve, J. Milbrandt, R. D. Mitra, Single-Cell RNA-Seq Uncovers a Robust Transcriptional Response to Morphine by Glia. *Cell Rep* **24**, 3619-3629 e3614 (2018).
145. R. Fan, L. M. Schrott, T. Arnold, S. Snelling, M. Rao, D. Graham, A. Cornelius, N. L. Korneeva, Chronic oxycodone induces axonal degeneration in rat brain. *BMC Neurosci* **19**, 15 (2018).
146. K. Bartus, N. D. James, K. D. Bosch, E. J. Bradbury, Chondroitin sulphate proteoglycans: key modulators of spinal cord and brain plasticity. *Exp Neurol* **235**, 5-17 (2012).
147. A. Beroun, S. Mitra, P. Michaluk, B. Pijet, M. Stefaniuk, L. Kaczmarek, MMPs in learning and memory and neuropsychiatric disorders. *Cell Mol Life Sci* **76**, 3207-3228 (2019).
148. N. Akhter, M. Nix, Y. Abdul, S. Singh, S. Husain, Delta-opioid receptors attenuate TNF-alpha-induced MMP-2 secretion from human ONH astrocytes. *Invest Ophthalmol Vis Sci* **54**, 6605-6611 (2013).
149. S. T. T. Schetters, D. Gomez-Nicola, J. J. Garcia-Vallejo, Y. Van Kooyk, Neuroinflammation: Microglia and T Cells Get Ready to Tango. *Front Immunol* **8**, 1905 (2017).
150. U. K. Hanisch, Microglia as a source and target of cytokines. *Glia* **40**, 140-155 (2002).
151. Y. Y. Chan, S. N. Yang, J. C. Lin, J. L. Chang, J. G. Lin, W. Y. Lo, Inflammatory response in heroin addicts undergoing methadone maintenance treatment. *Psychiatry Res* **226**, 230-234 (2015).
152. R. B. Lu, T. Y. Wang, S. Y. Lee, S. L. Chen, Y. H. Chang, P. See Chen, S. H. Lin, C. H. Chu, S. Y. Huang, N. S. Tzeng, I. H. Lee, K. Chin Chen, Y. Kuang Yang, P. Chen, S. H. Chen, J. S. Hong, Correlation between interleukin-6 levels and methadone maintenance therapy outcomes. *Drug Alcohol Depend* **204**, 107516 (2019).

1419 153. I. R. Holtman, D. Skola, C. K. Glass, Transcriptional control of microglia
1420 phenotypes in health and disease. *J Clin Invest* **127**, 3220-3229 (2017).
1421 154. C. Borner, J. Kraus, H. Schroder, H. Ammer, V. Hollt, Transcriptional regulation
1422 of the human mu-opioid receptor gene by interleukin-6. *Mol Pharmacol* **66**, 1719-
1423 1726 (2004).
1424 155. A. Dityatev, D. A. Rusakov, Molecular signals of plasticity at the tetrapartite
1425 synapse. *Curr Opin Neurobiol* **21**, 353-359 (2011).
1426 156. R. W. Yao, Y. Wang, L. L. Chen, Cellular functions of long noncoding RNAs. *Nat*
1427 *Cell Biol* **21**, 542-551 (2019).
1428 157. J. J. Lee, R. Wedow, A. Okbay, E. Kong, O. Maghzian, M. Zacher, T. A. Nguyen-
1429 Viet, P. Bowers, J. Sidorenko, R. Karlsson Linner, M. A. Fontana, T. Kundu, C.
1430 Lee, H. Li, R. Li, R. Royer, P. N. Timshel, R. K. Walters, E. A. Willoughby, L.
1431 Yengo, T. andMe Research, Cogent, C. Social Science Genetic Association, M.
1432 Alver, Y. Bao, D. W. Clark, F. R. Day, N. A. Furlotte, P. K. Joshi, K. E. Kemper,
1433 A. Kleinman, C. Langenberg, R. Magi, J. W. Trampush, S. S. Verma, Y. Wu, M.
1434 Lam, J. H. Zhao, Z. Zheng, J. D. Boardman, H. Campbell, J. Freese, K. M.
1435 Harris, C. Hayward, P. Herd, M. Kumari, T. Lencz, J. Luan, A. K. Malhotra, A.
1436 Metspalu, L. Milani, K. K. Ong, J. R. B. Perry, D. J. Porteous, M. D. Ritchie, M. C.
1437 Smart, B. H. Smith, J. Y. Tung, N. J. Wareham, J. F. Wilson, J. P. Beauchamp,
1438 D. C. Conley, T. Esko, S. F. Lehrer, P. K. E. Magnusson, S. Oskarsson, T. H.
1439 Pers, M. R. Robinson, K. Thom, C. Watson, C. F. Chabris, M. N. Meyer, D. I.
1440 Laibson, J. Yang, M. Johannesson, P. D. Koellinger, P. Turley, P. M. Visscher, D.
1441 J. Benjamin, D. Cesarini, Gene discovery and polygenic prediction from a
1442 genome-wide association study of educational attainment in 1.1 million
1443 individuals. *Nat Genet* **50**, 1112-1121 (2018).
1444 158. J. Mez, J. Chung, G. Jun, J. Kriegel, A. P. Bourlas, R. Sherva, M. W. Logue, L. L.
1445 Barnes, D. A. Bennett, J. D. Buxbaum, G. S. Byrd, P. K. Crane, N. Ertekin-Taner,
1446 D. Evans, M. D. Fallin, T. Foroud, A. Goate, N. R. Graff-Radford, K. S. Hall, M. I.
1447 Kamboh, W. A. Kukull, E. B. Larson, J. J. Manly, C. Alzheimer's Disease
1448 Genetics, J. L. Haines, R. Mayeux, M. A. Pericak-Vance, G. D. Schellenberg, K.
1449 L. Lunetta, L. A. Farrer, Two novel loci, COBL and SLC10A2, for Alzheimer's
1450 disease in African Americans. *Alzheimers Dement* **13**, 119-129 (2017).
1451 159. G. Steele-Perkins, C. Plachez, K. G. Butz, G. Yang, C. J. Bachurski, S. L.
1452 Kinsman, E. D. Litwack, L. J. Richards, R. M. Gronostajski, The transcription
1453 factor gene Nfib is essential for both lung maturation and brain development. *Mol*
1454 *Cell Biol* **25**, 685-698 (2005).
1455 160. L. das Neves, C. S. Duchala, F. Tolentino-Silva, M. A. Haxhiu, C. Colmenares,
1456 W. B. Macklin, C. E. Campbell, K. G. Butz, R. M. Gronostajski, Disruption of the
1457 murine nuclear factor I-A gene (Nfia) results in perinatal lethality, hydrocephalus,
1458 and agenesis of the corpus callosum. *Proc Natl Acad Sci U S A* **96**, 11946-11951
1459 (1999).
1460 161. I. Schanze, J. Bunt, J. W. C. Lim, D. Schanze, R. J. Dean, M. Alders, P.
1461 Blanchet, T. Attie-Bitach, S. Berland, S. Boogert, S. Boppudi, C. J. Bridges, M. T.
1462 Cho, W. B. Dobyns, D. Donnai, J. Douglas, D. L. Earl, T. J. Edwards, L. Faivre,
1463 B. Fregeau, D. Genevieve, M. Gerard, V. Gatinois, M. Holder-Espinasse, S. F.
1464 Huth, K. Izumi, B. Kerr, E. Lacaze, P. Lakeman, S. Mahida, G. M. Mirzaa, S. M.

1465 Morgan, C. Nowak, H. Peeters, F. Petit, D. T. Pilz, J. Puechberty, E. Reinstein, J.
1466 B. Riviere, A. B. Santani, A. Schneider, E. H. Sherr, C. Smith-Hicks, I. Wieland,
1467 E. Zackai, X. Zhao, R. M. Gronostajski, M. Zenker, L. J. Richards, NFIB
1468 Haploinsufficiency Is Associated with Intellectual Disability and Macrocephaly.
1469 *Am J Hum Genet* **103**, 752-768 (2018).
1470 162. I. Canals, A. Ginisty, E. Quist, R. Timmerman, J. Fritze, G. Miskinyte, E. Monni,
1471 M. G. Hansen, I. Hidalgo, D. Bryder, J. Bengzon, H. Ahlenius, Rapid and efficient
1472 induction of functional astrocytes from human pluripotent stem cells. *Nat*
1473 *Methods* **15**, 693-696 (2018).
1474 163. B. Lozzi, T. W. Huang, D. Sardar, A. Y. Huang, B. Deneen, Regionally Distinct
1475 Astrocytes Display Unique Transcription Factor Profiles in the Adult Brain. *Front*
1476 *Neurosci* **14**, 61 (2020).
1477 164. C. A. Hanlon, L. T. Dowdle, J. S. Henderson, Modulating Neural Circuits with
1478 Transcranial Magnetic Stimulation: Implications for Addiction Treatment
1479 Development. *Pharmacol Rev* **70**, 661-683 (2018).
1480 165. R. C. Bagot, H. M. Cates, I. Purushothaman, Z. S. Lorsch, D. M. Walker, J.
1481 Wang, X. Huang, O. M. Schlüter, I. Maze, C. J. Peña, E. A. Heller, O. Issler, M.
1482 Wang, W.-M. Song, J. L. Stein, X. Liu, M. A. Doyle, K. N. Scobie, H. S. Sun, R. L.
1483 Neve, D. Geschwind, Y. Dong, L. Shen, B. Zhang, E. J. Nestler, Circuit-wide
1484 Transcriptional Profiling Reveals Brain Region-Specific Gene Networks
1485 Regulating Depression Susceptibility. *Neuron* **90**, 969-983 (2016).
1486 166. D. M. Walker, H. M. Cates, Y. E. Loh, I. Purushothaman, A. Ramakrishnan, K. M.
1487 Cahill, C. K. Lardner, A. Godino, H. G. Kronman, J. Rabkin, Z. S. Lorsch, P.
1488 Mews, M. A. Doyle, J. Feng, B. Labonte, J. W. Koo, R. C. Bagot, R. W. Logan,
1489 M. L. Seney, E. S. Calipari, L. Shen, E. J. Nestler, Cocaine Self-administration
1490 Alters Transcriptome-wide Responses in the Brain's Reward Circuitry. *Biol*
1491 *Psychiatry* **84**, 867-880 (2018).
1492 167. A. Torres, A. Catena, A. Megias, A. Maldonado, A. Candido, A. Verdejo-Garcia,
1493 J. C. Perales, Emotional and non-emotional pathways to impulsive behavior and
1494 addiction. *Front Hum Neurosci* **7**, 43 (2013).
1495 168. M. J. Kreek, D. A. Nielsen, E. R. Butelman, K. S. LaForge, Genetic influences on
1496 impulsivity, risk taking, stress responsivity and vulnerability to drug abuse and
1497 addiction. *Nat Neurosci* **8**, 1450-1457 (2005).
1498 169. L. Rodriguez-Cintas, C. Daigre, L. Grau-Lopez, C. Barral, J. Perez-Pazos, N.
1499 Voltes, M. D. Braquehais, M. Casas, C. Roncero, Impulsivity and addiction
1500 severity in cocaine and opioid dependent patients. *Addict Behav* **58**, 104-109
1501 (2016).
1502 170. C. A. Winstanley, The orbitofrontal cortex, impulsivity, and addiction: probing
1503 orbitofrontal dysfunction at the neural, neurochemical, and molecular level. *Ann*
1504 *N Y Acad Sci* **1121**, 639-655 (2007).
1505 171. J. R. Glausier, M. A. Kelly, S. Salem, K. Chen, D. A. Lewis, Proxy measures of
1506 premortem cognitive aptitude in postmortem subjects with schizophrenia.
1507 *Psychol. Med.*, 1-8 (2019).
1508 172. J. K. Mai, M. Majtanik, G. Paxinos, Atlas of the human brain. (2016).
1509 173. T. Hashimoto, H. H. Bazmi, K. Mirnics, Q. Wu, A. R. Sampson, D. A. Lewis,
1510 Conserved regional patterns of GABA-related transcript expression in the

1511 neocortex of subjects with schizophrenia. *The American Journal of Psychiatry*
1512 **165**, 479-489 (2008).
1513 174. D. W. Volk, T. Matsubara, S. Li, E. J. Sengupta, D. Georgiev, Y. Minabe, A.
1514 Sampson, T. Hashimoto, D. A. Lewis, Deficits in transcriptional regulators of
1515 cortical parvalbumin neurons in schizophrenia. *Am. J. Psychiatry* **169**, 1082-1091
1516 (2012).
1517 175. M. Pertea, D. Kim, G. M. Pertea, J. T. Leek, S. L. Salzberg, Transcript-level
1518 expression analysis of RNA-seq experiments with HISAT, StringTie and
1519 Ballgown. *Nat Protoc* **11**, 1650-1667 (2016).
1520 176. S. Anders, P. T. Pyl, W. Huber, HTSeq--a Python framework to work with high-
1521 throughput sequencing data. *Bioinformatics* **31**, 166-169 (2015).
1522 177. C. W. Law, Y. Chen, W. Shi, G. K. Smyth, voom: Precision weights unlock linear
1523 model analysis tools for RNA-seq read counts. *Genome Biol* **15**, R29 (2014).
1524 178. M. E. Ritchie, B. Phipson, D. Wu, Y. Hu, C. W. Law, W. Shi, G. K. Smyth, limma
1525 powers differential expression analyses for RNA-sequencing and microarray
1526 studies. *Nucleic Acids Res* **43**, e47 (2015).
1527 179. M. L. Seney, Z. Huo, K. Cahill, L. French, R. Puralewski, J. Zhang, R. W. Logan,
1528 G. Tseng, D. A. Lewis, E. Sibille, Opposite Molecular Signatures of Depression in
1529 Men and Women. *Biol Psychiatry* **84**, 18-27 (2018).
1530 180. X. Wang, Y. Lin, C. Song, E. Sibille, G. C. Tseng, Detecting disease-associated
1531 genes with confounding variable adjustment and the impact on genomic meta-
1532 analysis: with application to major depressive disorder. *BMC Bioinformatics* **13**,
1533 52 (2012).
1534 181. Y. Benjamini, Y. Hochberg, Controlling the false discovery rate: a practical
1535 approach to multiple testing. *Journal of the Royal Statistical Society: Series B* **57**,
1536 289-300 (1995).
1537 182. B. Labonté, O. Engmann, I. Purushothaman, C. Menard, J. Wang, C. Tan, J. R.
1538 Scarpa, G. Moy, Y.-H. E. Loh, M. Cahill, Z. S. Lorsch, P. J. Hamilton, E. S.
1539 Calipari, G. E. Hodes, O. Issler, H. Kronman, M. Pfau, A. L. J. Obradovic, Y.
1540 Dong, R. L. Neve, S. Russo, A. Kazarskis, C. Tamminga, N. Mechawar, G.
1541 Turecki, B. Zhang, L. Shen, E. J. Nestler, Sex-specific transcriptional signatures
1542 in human depression. *Nat. Med.* **23**, 1102-1111 (2017).
1543 183. W. Paden, K. Barko, R. Puralewski, K. M. Cahill, Z. Huo, M. A. Shelton, G. C.
1544 Tseng, R. W. Logan, M. L. Seney, Sex differences in adult mood and in stress-
1545 induced transcriptional coherence across mesocorticolimbic circuitry. *Transl*
1546 *Psychiatry* **10**, 59 (2020).
1547 184. P. Moulos, P. Hatzis, Systematic integration of RNA-Seq statistical algorithms for
1548 accurate detection of differential gene expression patterns. *Nucleic Acids Res* **43**,
1549 e25 (2015).
1550 185. W. J. Kent, C. W. Sugnet, T. S. Furey, K. M. Roskin, T. H. Pringle, A. M. Zahler,
1551 D. Haussler, The human genome browser at UCSC. *Genome Res* **12**, 996-1006
1552 (2002).
1553 186. A. D. Yates, P. Achuthan, W. Akanni, J. Allen, J. Allen, J. Alvarez-Jarreta, M. R.
1554 Amode, I. M. Armean, A. G. Azov, R. Bennett, J. Bhai, K. Billis, S. Boddu, J. C.
1555 Marugan, C. Cummins, C. Davidson, K. Dodiya, R. Fatima, A. Gall, C. G. Giron,
1556 L. Gil, T. Grego, L. Haggerty, E. Haskell, T. Hourlier, O. G. Izuogu, S. H.

1557 Janacek, T. Juettemann, M. Kay, I. Lavidas, T. Le, D. Lemos, J. G. Martinez, T.
1558 Maurel, M. McDowall, A. McMahon, S. Mohanan, B. Moore, M. Nuhn, D. N.
1559 Oheh, A. Parker, A. Parton, M. Patricio, M. P. Sakthivel, A. I. Abdul Salam, B. M.
1560 Schmitt, H. Schuilenburg, D. Sheppard, M. Sycheva, M. Szuba, K. Taylor, A.
1561 Thormann, G. Threadgold, A. Vullo, B. Walts, A. Winterbottom, A. Zadissa, M.
1562 Chakiachvili, B. Flint, A. Frankish, S. E. Hunt, I. I. G, M. Kostadima, N. Langridge,
1563 J. E. Loveland, F. J. Martin, J. Morales, J. M. Mudge, M. Muffato, E. Perry, M.
1564 Ruffier, S. J. Trevanion, F. Cunningham, K. L. Howe, D. R. Zerbino, P. Flicek,
1565 Ensembl 2020. *Nucleic Acids Res* **48**, D682-D688 (2020).
1566 187. B. Zhang, S. Horvath, A general framework for weighted gene co-expression
1567 network analysis. *Stat Appl Genet Mol Biol* **4**, Article17 (2005).
1568 188. P. Langfelder, B. Zhang, S. Horvath, Defining clusters from a hierarchical cluster
1569 tree: the Dynamic Tree Cut package for R. *Bioinformatics* **24**, 719-720 (2008).
1570 189. P. Langfelder, R. Luo, M. C. Oldham, S. Horvath, Is my network module
1571 preserved and reproducible? *PLoS Comput Biol* **7**, e1001057 (2011).
1572 190. B. Zhang, C. Gaiteri, L. G. Bodea, Z. Wang, J. McElwee, A. A. Podtelezhnikov,
1573 C. Zhang, T. Xie, L. Tran, R. Dobrin, E. Fluder, B. Clurman, S. Melquist, M.
1574 Narayanan, C. Suver, H. Shah, M. Mahajan, T. Gillis, J. Mysore, M. E.
1575 MacDonald, J. R. Lamb, D. A. Bennett, C. Molony, D. J. Stone, V. Gudnason, A.
1576 J. Myers, E. E. Schadt, H. Neumann, J. Zhu, V. Emilsson, Integrated systems
1577 approach identifies genetic nodes and networks in late-onset Alzheimer's
1578 disease. *Cell* **153**, 707-720 (2013).
1579 191. A. A. Margolin, I. Nemenman, K. Basso, C. Wiggins, G. Stolovitzky, R. Dalla
1580 Favera, A. Califano, ARACNE: an algorithm for the reconstruction of gene
1581 regulatory networks in a mammalian cellular context. *BMC Bioinformatics* **7**
1582 **Suppl 1**, S7 (2006).
1583 192. S. B. Plaisier, R. Taschereau, J. A. Wong, T. G. Graeber, Rank-rank
1584 hypergeometric overlap: identification of statistically significant overlap between
1585 gene-expression signatures. *Nucleic Acids Res* **38**, e169 (2010).
1586 193. K. M. Cahill, Z. Huo, G. C. Tseng, R. W. Logan, M. L. Seney, Improved
1587 identification of concordant and discordant gene expression signatures using an
1588 updated rank-rank hypergeometric overlap approach. *Sci Rep* **8**, 9588 (2018).
1589 194. Y. Zhong, Y. W. Wan, K. Pang, L. M. Chow, Z. Liu, Digital sorting of complex
1590 tissues for cell type-specific gene expression profiles. *BMC Bioinformatics* **14**, 89
1591 (2013).
1592 195. A. T. McKenzie, M. Wang, M. E. Hauberg, J. F. Fullard, A. Kozlenkov, A.
1593 Keenan, Y. L. Hurd, S. Dracheva, P. Casaccia, P. Roussos, B. Zhang, Brain Cell
1594 Type Specific Gene Expression and Co-expression Network Architectures. *Sci*
1595 *Rep* **8**, 8868 (2018).
1596 196. H. K. Finucane, Y. A. Reshef, V. Anttila, K. Slowikowski, A. Gusev, A. Byrnes, S.
1597 Gazal, P. R. Loh, C. Lareau, N. Shoresh, G. Genovese, A. Saunders, E.
1598 Macosko, S. Pollack, C. Brainstorm, J. R. B. Perry, J. D. Buenrostro, B. E.
1599 Bernstein, S. Raychaudhuri, S. McCarroll, B. M. Neale, A. L. Price, Heritability
1600 enrichment of specifically expressed genes identifies disease-relevant tissues
1601 and cell types. *Nat Genet* **50**, 621-629 (2018).

197. B. K. Bulik-Sullivan, P. R. Loh, H. K. Finucane, S. Ripke, J. Yang, C. Schizophrenia Working Group of the Psychiatric Genomics, N. Patterson, M. J. Daly, A. L. Price, B. M. Neale, LD Score regression distinguishes confounding from polygenicity in genome-wide association studies. *Nat Genet* **47**, 291-295 (2015).
198. K. J. A. Johnston, M. J. Adams, B. I. Nicholl, J. Ward, R. J. Strawbridge, A. Ferguson, A. M. McIntosh, M. E. S. Bailey, D. J. Smith, Genome-wide association study of multisite chronic pain in UK Biobank. *PLoS Genet* **15**, e1008164 (2019).
199. C. Schizophrenia Working Group of the Psychiatric Genomics, Biological insights from 108 schizophrenia-associated genetic loci. *Nature* **511**, 421-427 (2014).
200. Z. Cheng, H. Zhou, R. Sherva, L. A. Farrer, H. R. Kranzler, J. Gelernter, Genome-wide Association Study Identifies a Regulatory Variant of RGMA Associated With Opioid Dependence in European Americans. *Biol Psychiatry* **84**, 762-770 (2018).
201. J. A. Pasman, K. J. H. Verweij, Z. Gerring, S. Stringer, S. Sanchez-Roige, J. L. Treur, A. Abdellaoui, M. G. Nivard, B. M. L. Baselmans, J. S. Ong, H. F. Ip, M. D. van der Zee, M. Bartels, F. R. Day, P. Fontanillas, S. L. Elson, T. andMe Research, H. de Wit, L. K. Davis, J. MacKillop, C. Substance Use Disorders Working Group of the Psychiatric Genomics, C. International Cannabis, J. L. Derringer, S. J. T. Branje, C. A. Hartman, A. C. Heath, P. A. C. van Lier, P. A. F. Madden, R. Magi, W. Meeus, G. W. Montgomery, A. J. Oldehinkel, Z. Pausova, J. A. Ramos-Quiroga, T. Paus, M. Ribases, J. Kaprio, M. P. M. Boks, J. T. Bell, T. D. Spector, J. Gelernter, D. I. Boomsma, N. G. Martin, S. MacGregor, J. R. B. Perry, A. A. Palmer, D. Posthuma, M. R. Munafo, N. A. Gillespie, E. M. Derks, J. M. Vink, GWAS of lifetime cannabis use reveals new risk loci, genetic overlap with psychiatric traits, and a causal influence of schizophrenia. *Nat Neurosci* **21**, 1161-1170 (2018).
202. C. International Obsessive Compulsive Disorder Foundation Genetics, O. C. D. C. G. A. Studies, Revealing the complex genetic architecture of obsessive-compulsive disorder using meta-analysis. *Mol Psychiatry* **23**, 1181-1188 (2018).
203. H. S. Dashti, S. E. Jones, A. R. Wood, J. M. Lane, V. T. van Hees, H. Wang, J. A. Rhodes, Y. Song, K. Patel, S. G. Anderson, R. N. Beaumont, D. A. Bechtold, J. Bowden, B. E. Cade, M. Garaulet, S. D. Kyle, M. A. Little, A. S. Loudon, A. I. Luik, F. Scheer, K. Spiegelhalder, J. Tyrrell, D. J. Gottlieb, H. Tiemeier, D. W. Ray, S. M. Purcell, T. M. Frayling, S. Redline, D. A. Lawlor, M. K. Rutter, M. N. Weedon, R. Saxena, Genome-wide association study identifies genetic loci for self-reported habitual sleep duration supported by accelerometer-derived estimates. *Nat Commun* **10**, 1100 (2019).
204. M. C. Zillikens, S. Demissie, Y. H. Hsu, L. M. Yerges-Armstrong, W. C. Chou, L. Stolk, G. Livshits, L. Broer, T. Johnson, D. L. Koller, Z. Kutalik, J. Luan, I. Malkin, J. S. Ried, A. V. Smith, G. Thorleifsson, L. Vandenput, J. Hua Zhao, W. Zhang, A. Aghdassi, K. Akesson, N. Amin, L. J. Baier, I. Barroso, D. A. Bennett, L. Bertram, R. Biffar, M. Bochud, M. Boehnke, I. B. Borecki, A. S. Buchman, L. Byberg, H. Campbell, N. Campos Obanda, J. A. Cauley, P. M. Cawthon, H. Cederberg, Z. Chen, N. H. Cho, H. Jin Choi, M. Claussnitzer, F. Collins, S. R.

Cummings, P. L. De Jager, I. Demuth, R. A. M. Dhonukshe-Rutten, L. Diatchenko, G. Eiriksdottir, A. W. Enneman, M. Erdos, J. G. Eriksson, J. Eriksson, K. Estrada, D. S. Evans, M. F. Feitosa, M. Fu, M. Garcia, C. Gieger, T. Girke, N. L. Glazer, H. Grallert, J. Grewal, B. G. Han, R. L. Hanson, C. Hayward, A. Hofman, E. P. Hoffman, G. Homuth, W. C. Hsueh, M. J. Hubal, A. Hubbard, K. M. Huffman, L. B. Husted, T. Illig, E. Ingelsson, T. Ittermann, J. O. Jansson, J. M. Jordan, A. Jula, M. Karlsson, K. T. Khaw, T. O. Kilpelainen, N. Klopp, J. S. L. Kloth, H. A. Koistinen, W. E. Kraus, S. Kritchevsky, T. Kuulasmaa, J. Kuusisto, M. Laakso, J. Lahti, T. Lang, B. L. Langdahl, L. J. Launer, J. Y. Lee, M. M. Lerch, J. R. Lewis, L. Lind, C. Lindgren, Y. Liu, T. Liu, Y. Liu, O. Ljunggren, M. Lorentzon, R. N. Luben, W. Maixner, F. E. McGuigan, C. Medina-Gomez, T. Meitinger, H. Melhus, D. Mellstrom, S. Melov, K. Michaelsson, B. D. Mitchell, A. P. Morris, L. Mosekilde, A. Newman, C. M. Nielson, J. R. O'Connell, B. A. Oostra, E. S. Orwoll, A. Palotie, S. C. J. Parker, M. Peacock, M. Perola, A. Peters, O. Polasek, R. L. Prince, K. Raikkonen, S. H. Ralston, S. Ripatti, J. A. Robbins, J. I. Rotter, I. Rudan, V. Salomaa, S. Satterfield, E. E. Schadt, S. Schipf, L. Scott, J. Sehmi, J. Shen, C. Soo Shin, G. Sigurdsson, S. Smith, N. Soranzo, A. Stancakova, E. Steinhagen-Thiessen, E. A. Streeten, U. Styrkarsdottir, K. M. A. Swart, S. T. Tan, M. A. Tarnopolsky, P. Thompson, C. A. Thomson, U. Thorsteinsdottir, E. Tikkanen, G. J. Tranah, J. Tuomilehto, N. M. van Schoor, A. Verma, P. Vollenweider, H. Volzke, J. Wactawski-Wende, M. Walker, M. N. Weedon, R. Welch, H. E. Wichmann, E. Widen, F. M. K. Williams, J. F. Wilson, N. C. Wright, W. Xie, L. Yu, Y. Zhou, J. C. Chambers, A. Doring, C. M. van Duijn, M. J. Econs, V. Gudnason, J. S. Kooner, B. M. Psaty, T. D. Spector, K. Stefansson, F. Rivadeneira, A. G. Uitterlinden, N. J. Wareham, V. Ossowski, D. Waterworth, R. J. F. Loos, D. Karasik, T. B. Harris, C. Ohlsson, D. P. Kiel, Large meta-analysis of genome-wide association studies identifies five loci for lean body mass. *Nat Commun* **8**, 80 (2017).

205. J. P. Kemp, J. A. Morris, C. Medina-Gomez, V. Forgetta, N. M. Warrington, S. E. Youlten, J. Zheng, C. L. Gregson, E. Grundberg, K. Trajanoska, J. G. Logan, A. S. Pollard, P. C. Sparkes, E. J. Ghirardello, R. Allen, V. D. Leitch, N. C. Butterfield, D. Komla-Ebri, A. T. Adoum, K. F. Curry, J. K. White, F. Kussy, K. M. Greenlaw, C. Xu, N. C. Harvey, C. Cooper, D. J. Adams, C. M. T. Greenwood, M. T. Maurano, S. Kaptoge, F. Rivadeneira, J. H. Tobias, P. I. Croucher, C. L. Ackert-Bicknell, J. H. D. Bassett, G. R. Williams, J. B. Richards, D. M. Evans, Identification of 153 new loci associated with heel bone mineral density and functional involvement of GPC6 in osteoporosis. *Nat Genet* **49**, 1468-1475 (2017).

206. J. M. M. Howson, W. Zhao, D. R. Barnes, W. K. Ho, R. Young, D. S. Paul, L. L. Waite, D. F. Freitag, E. B. Fauman, E. L. Salfati, B. B. Sun, J. D. Eicher, A. D. Johnson, W. H. H. Sheu, S. F. Nielsen, W. Y. Lin, P. Surendran, A. Malarstig, J. B. Wilk, A. Tybjaerg-Hansen, K. L. Rasmussen, P. R. Kamstrup, P. Deloukas, J. Erdmann, S. Kathiresan, N. J. Samani, H. Schunkert, H. Watkins, CardioGramplusC4D, R. Do, D. J. Rader, J. A. Johnson, S. L. Hazen, A. A. Quyyumi, J. A. Spertus, C. J. Pepine, N. Franceschini, A. Justice, A. P. Reiner, S. Buyske, L. A. Hindorff, C. L. Carty, K. E. North, C. Kooperberg, E. Boerwinkle,

K. Young, M. Graff, U. Peters, D. Absher, C. A. Hsiung, W. J. Lee, K. D. Taylor, Y. H. Chen, I. T. Lee, X. Guo, R. H. Chung, Y. J. Hung, J. I. Rotter, J. J. Juang, T. Quertermous, T. D. Wang, A. Rasheed, P. Frossard, D. S. Alam, A. A. S. Majumder, E. Di Angelantonio, R. Chowdhury, C. V. D. Epic, Y. I. Chen, B. G. Nordestgaard, T. L. Assimes, J. Danesh, A. S. Butterworth, D. Saleheen, Fifteen new risk loci for coronary artery disease highlight arterial-wall-specific mechanisms. *Nat Genet* **49**, 1113-1119 (2017).

1703 **Acknowledgments:** We would like to thank the staff and technicians who work diligently
1704 as part of the Brain Tissue Program at the University of Pittsburgh. Human tissue was
1705 obtained from the NIH NeuroBioBank and the University of Pittsburgh Brain Tissue
1706 Donation Program. This study was funded by the Hamilton Family Prize for Basic
1707 Neuroscience Research in Psychiatry at the University of Pittsburgh School of Medicine
1708 to R.W.L., NHLBI R01HL150432 to R.W.L, and NIDA R01DA051390 to R.W.L and M.L.S.

1709

1710 **Author Contributions:** M.L.S., J.R.G., D.A.L., G.C.T. and R.W.L. designed and
1711 coordinated the study. X.X., W.Z., J.W., B.N.P., C.S., A.R.P., Z.F., G.C.T., and R.W.L.
1712 conducted statistical analysis and data interpretation. S.M.K., M.A.H., J.R.G., and M.A.S.
1713 obtained samples and processed samples for RNA-sequencing. M.L.S. and R.W.L.
1714 obtained funding for the project, and M.L.S., Z.F., and R.W.L. drafted the manuscript.

1715

1716 **Competing Interests:** None.

1717

1718